Universität Bonn

Physikalisches Institut

STYX Experiment: Further development

Elena Zarkh

This thesis is concentrating on improving and developing of STYX which is an experiment of the obligatory laboratory course at the physics department of Bonn University. The experiment was built from decommissioned ZEUS detector at DESY and studies muons from the secondary cosmic rays, analyses their distribution at sea-level and gives students an opportunity to work with detector techniques as used in current particle physics experiments such as ATLAS at CERN. After close examination of the experiment two main tasks were decided: reshaping of software and testing and extension of the detector setup. For the first task refactoring of the code was performed, making reconstruction of muon tracks more precise, the code readable and more flexible for future changes. For the second task the electronic elements of the experiment were tested and, if possible, exchanged or repaired. In next step the setup was extended with an additional module - a straw tube detector - to allow new studies on efficiency of the experiment. In general, a big step in improving experiment was done creating new possible tasks for students.

Physikalisches Institut der
Universität Bonn
Nussallee 12
D-53115 Bonn

BONN-IB-2015-02
January 2015

Universität Bonn

Physikalisches Institut

STYX Experiment: Further development

Elena Zarkh

Dieser Forschungsbericht wurde als Masterarbeit von der Mathematisch-Naturwissenschaftlichen Fakultät der Universität Bonn angenommen.

Angenommen am: 30.01.2015
1. Gutachter: Prof. Dr. Ian C. Brock
2. Gutachter: Priv.Doz. Dr. Philip Bechtle

For my grandmother.

Contents

CHAPTER 1

Introduction

Never doubt that a small group of thoughtful, committed, citizens can change the world. Indeed, it is the only thing that ever has.

-Margaret Mead

STYX (Straw Tube Young students eXperiment) is an experiment in the students' laboratory course of the University of Bonn. STYX is a relatively new experiment and was started only a few years ago as a joint project of two experimental physics groups, Desch and Brock. Built from the modules of STT (straw tube tracker) of the ZEUS experiment at HERA, the first prototype is located at CERN, in Switzerland. Shortly after, the same experiment was built in Bonn and included in the laboratory course.

Muons from secondary cosmic rays are the particles studied with STYX. Cosmic rays are particles which are coming from outer space. Different objects are assumed to be possible sources of the high energetic cosmic rays, for example, AGNs (Active Galactic Nuclei), supernovae and the galactic center[1]. There are probably also other sources, but as the original particles decay in the atmosphere and through the disturbance through the magnetic fields of our Sun, Earth and also of the intergalactic and galactic objects direct studies are impossible.

The experiment aims to provide a basic understanding of the cosmic radiation, gas detectors, tracking of charged particles, readout electronics and computer-based data analysis. STYX is a small detector which detects the muons at sea level. It measures the drift times of the particle and provides information on it for analysis. The data is first stored on a harddisk and then converted to a file type that can be processed with a PC. The experiment starts with a calibration of the detector. Calibration is described in more details in chapter 4.1.1. In the next step reconstruction and analysis of calibrated data can be executed. Reconstruction reconstructs step-by-step a track of the charged particle which passed the detector. Each step of the reconstrcution is explaind in chapter 3.4.3. Using information from the reconstruction the histogramms containing the angular distribution of tracks, number of registered events or hits(reconstructed drift circles) per event can be created. A further aim of the experiment is to verify the expected angular distribution for cosmic muons.

Teaching of the students is very important task at the university. Lectures are suppose to wake their interest in one or another specific field of their studies. In physics the laboratory courses play an essential role to inspire the students to choose their specialization. With that in mind the developments of the experiment should aim to improve STYX in a way, that performing the experiments would catch the students' interest.

This thesis first concentrates on studying the experiment and investigating possible improvements. The next chapter concentrates on the physics used in STYX. A short introduction to cosmic rays and an explanation of the working principals of gaseous detectors, scintillators and phtomoultipliers are presented. Chapter 3 explains the structure of the experiment, describes the setup and electronics and gives a brief description of the software used in STYX. Chapter 4 introduces the experiment in more detail, explaining the steps needed to perform the experiment and how the software works. After the first studies of STYX, the conclusions about possible developments are gathered in order to establish a plan for the improvements. The following two chapters describe the performed changes and developments in hardware and software of the experiment. In the last chapter the results of performed developments are summarized.

CHAPTER 2

Physics behind STYX

Every experiment is expected to test ansd study a theory based on earlier observations or predictions. And each experiment has to use different elements, electronic and technical devices, detectors. STYX concentrates on muons from secondary cosmic rays and uses gaseous detectors and a combination of a scintillator and a photomultiplier as a trigger system to gather more information about angular distribution of muons tracks at sea level. All the elements used in the experiment and its working principal will be explained in this chapter.

2.1 Cosmic rays

Cosmic rays are a flux of charged particles coming from space which interact with the molecules and atoms when reaching the Earth's atmosphere. The energies of cosmic rays range between 10^{-3} eV and 10^{20}eV and the particles are coming from different sources, e.g. active galactic nuclei (AGNs), the Sun as well as other intra- or even extra-galactic stars. The studies of cosmic rays date back to the 1900s when the physicists observed strange radiation on the instruments isolated from other kinds of known radiation. The origin of this radiation was thought to be coming from the Earth's crust or even more below. However, Victor Hess in 1912 proved that the radiation was increasing with altitude [2] and accordingly was coming from above. In 1936 V. Hess received the Nobel Prize for the discovery of the cosmic rays.

Cosmic rays are divided into two categories, primary and secondary cosmic rays. Primary cosmic rays are the protons, nuclei and alpha particles. The secondary cosmic rays are the products of primary particles after the interaction with the atmosphere. Possible products after these interactions are presented in figure 2.1. Primary particles interact with atmosphere in the way that in most cases kaons or pions are produced. These then decay via following decay chains:

$$\begin{aligned} K^- &\rightarrow \pi^- + \pi^0, \quad K^+ \rightarrow \pi^+ + \pi^0 \\ K^- &\rightarrow \mu^- + \bar{\nu}_\mu, \quad K^+ \rightarrow \mu^+ + \nu_\mu \\ \pi^- &\rightarrow \mu^- + \bar{\nu}_\mu, \quad \pi^+ \rightarrow \mu^+ + \nu_\mu \end{aligned} \tag{2.1}$$

Charged pions decay further to muons or, more rarely, to electrons; neutral pions decay to photons. From some of the muons and photons electrons and positrons can be produced via pair production. Those electrons form an electromagnetic component of the cosmic rays and can be detected by mea-

suring Cherenkov radiation at sea level. Other components of the secondary cosmic rays at sea level are hadronic components (consisted of the primary cosmic particles after the interaction) and muonic component, which consists from the muons produced by decaying charged pions and which are studied by STYX experiment.

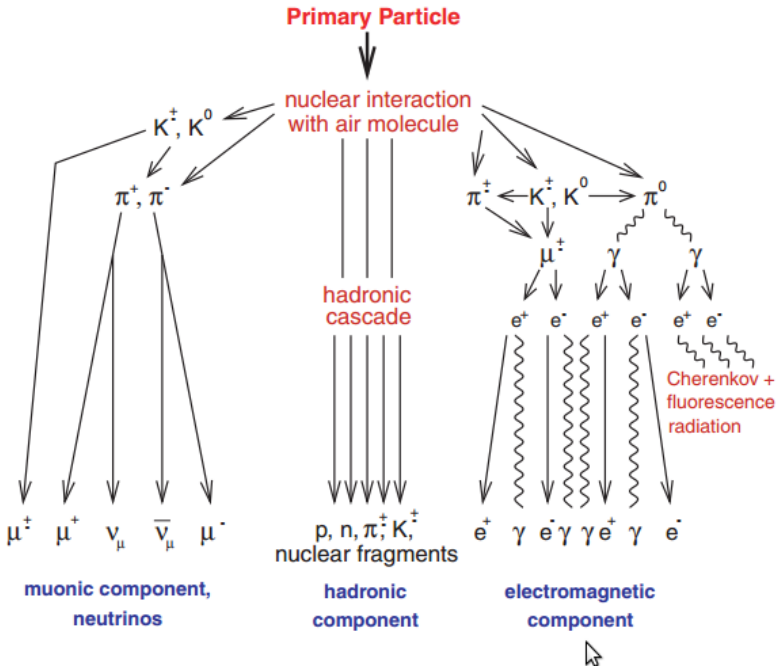

Figure 2.1: Scheme of the interaction of the cosmic rays with the atmosphere and possible decay products [3].

To determine the exact source of the primary cosmic rays is very difficult as the charged particle's trajectory is strongly influenced by cosmic objects, other particles or solar winds and the magnetic field of Earth. That makes it almost impossible to say from which direction exactly the particle came from.

The end products of the muonic component are muons, neutrinos and electrons. Muons present ≈80% of the charged component of secondary cosmic rays at sea level. The remaining almost 20% are mostly the electrons and positrons from the cascade, but also hadrons like nucleons, kaons and pions from the hadronic component of the cosmic rays. One would expect a flat angular distribution of the muons at sea level, but due to effects such as thickness of the atmosphere for different incident angle of the muon the distribution is predicted to look like that in the figure 2.3. Figure 2.2 shows the momentum distribution of muons at sea level. This effect varies depending on where on the Earth's surface the measurements are taken, e.g if the detector is placed higher or lower altitudes than sea level.

As not all about the cosmic rays can be written in one chapter further information can be found in "Astroparticle physics" by C.Gruppen [1] as well as PDG [4] or "Instruments and Methods for the Radio Detection of High Energy Cosmic Rays" by F.G.Schröder [3].

2.2 Gaseous detectors

The first gaseous ionization detectors were developed in the 1940s, but the first prototype was already used in 1908 which was able to register the α-particles [6, 7]. All gaseous detectors have the same basic construction shown in the figure 2.4, a cylindrical container with conductive walls filled with gas and a

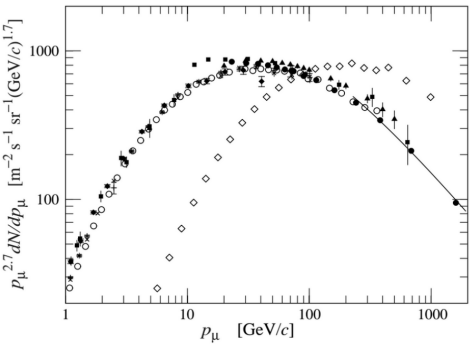

Figure 2.2: Momentum distribution of secondary cosmic ray muons at sea level from PDG [4]. Spectrum of muons at $\theta = 0°$ (⧫, ■, ▲, ▼, ×, +, ○, ●) and $\theta = 75°$ (◊).

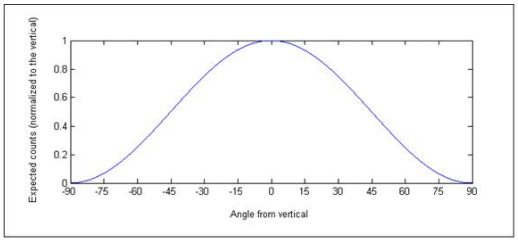

Figure 2.3: Angular distribution of secondary cosmic ray muons at sea level from a project of the University of Minnesota [5] .

thin wire. To the walls a negative (cathode) and to the wire (anode) a positive voltage is applied, so that an electrical field is established. When a charged particle passes through the tube, it creates electron-ion pairs. The electrical field in the tube causes the electrons and ions to drift to the anode or cathode, respectvely.

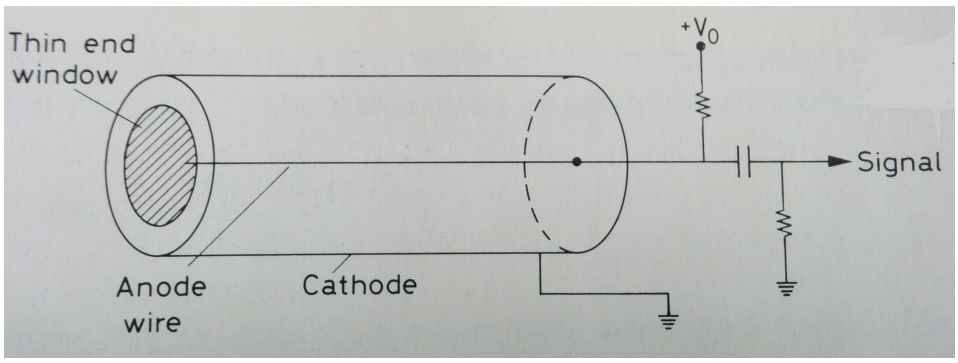

Figure 2.4: Scheme of the simple gas ionization detector [6].

In figure 2.5 the number of measured ions is shown as a function of voltage. The curve is divided into four areas depending on the applied voltage. In the first region no ions are measured as the voltage is too low and electron-ion pairs recombine shortly after ionization. The second region is the region where the ionization chambers operate. The voltage is high enough that the ion-electron pairs cannot recombine, a small current can be detected. In the next area the voltage is so high that the strength of the electric filed is high enough to accelerate the electrons, which now have enough energy to ionize the gas molecules in the tube. The new electrons are accelerated again and an electron avalanche is formed. The electric field is highest next to the anode, that means the avalanche occurs within a few radii of the wire. The resulting current is directly proportional to the original signal with amplification depending on the applied voltage, for this reason detectors operating in this region are called proportional chambers [6].

If the voltage is increased further, there is a point after which the proportionality of the current to signal is lost. It happens due to the gas molecules emitting photons which again interact with gas and create more electrons. The electrons can cause secondary avalanches to start. The measured signal is now not proportional to the original signal and after reaching saturation cannot give any information on

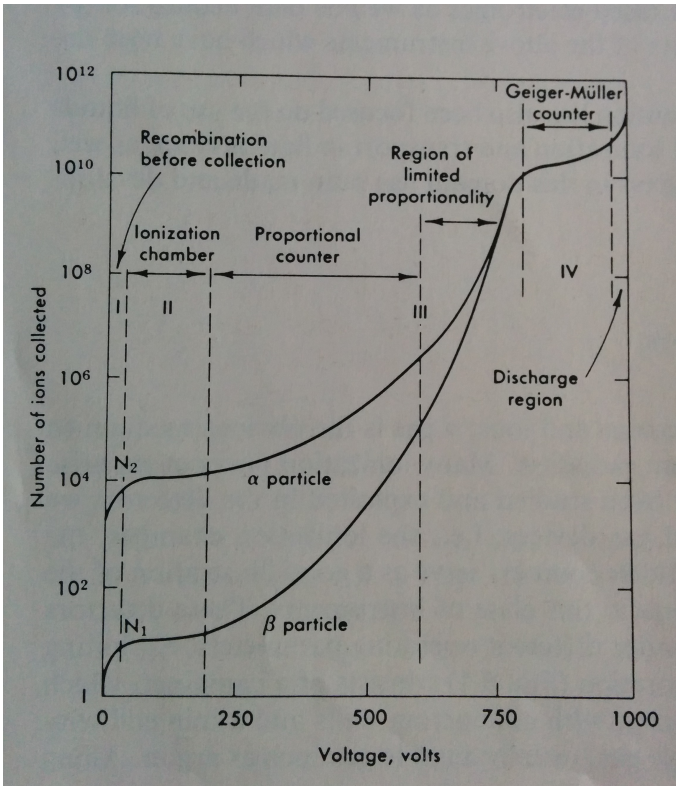

Figure 2.5: The total charge collected as a function of voltage in a single wire chamber [6].

the initial event anymore.To prevent this, a quenching gas can be used to absorb the photons. From this point the Geiger-Müller or breakdown counters are used. After this region the voltage should not be increased any further as the detector can be damaged because of continuous discharge in the gas [7].

2.2.1 Gas mixture

The main component of a gaseous detector is a gas or a gas mixture. It should be chosen considering following requirements: low working voltage, high proportionality and high gain. Argon (Ar) is often used for this purposes because it has a low working voltage and a high specific ionization to create possibly many electron-ion pairs at low voltage, but also is low priced compared to other noble gases, which have the same characteristics. As pure Ar at the high enough voltage starts to emit further photons and destroy the proportionality of the particle energy to signal a gas mixture is usually used. The quenching gas can be of organic or inorganic nature. The organic quenchers form solid or liquid polymers after some amount of a radiation has been absorbed. Those polymers can accumulate around the wire or the tube and the ions cannot be absorbed fast enough. The problem is that the radius of the wire or tube changes and that leads to decrease of the electric filed. The solution is to use inorganic quenchers, which are less effective but do not form the polymers. CO_2 as inorganic and CH_4 as organic gases are often used as the quenchers [6, 8].

2.3 Drift velocity and time

Drift velocity is the average velocity of the electrons or ions in the detector created by the charged particles passing through the detector. In the presence of the electric field the electrons and ions are accelerated to the anode or cathode respectively. The average velocity is decreased due to interruptions by the collisions with the molecules of the gas. As the electrons have a smaller mass then the ions, they can reach a higher drift velocity. The drift velocity is very important for gaseous detectors as the track position is calculated from the drift time and which can be calculated using the drift velocity.

2.4 Photomultipliers and scintillators

Scintillators combined with photomultipliers are often used as trigger systems and for time measurements components in an experiment because of their properties. PMTs have a fast time response which makes them most suited for the triggering and are sensitive to the applied energies, that means that the threshold to reduce the noise can be chosen precisely. The simple setup of such a detector is shown in the figure 2.6.

The first proposal of a device similar to a photomultiplier tube (PMT) was registered in the 1930s. L.A. Kubetzky found a new method to amplify a weak photocurrent. This tube already used a photocathode and a row of dynodes to multiply the electrons. But the construction was not as efficient [9] as PMTs used today. However, officially it was Zworykin et al. who developed the currently used version of the PMTs in 1939 [10].

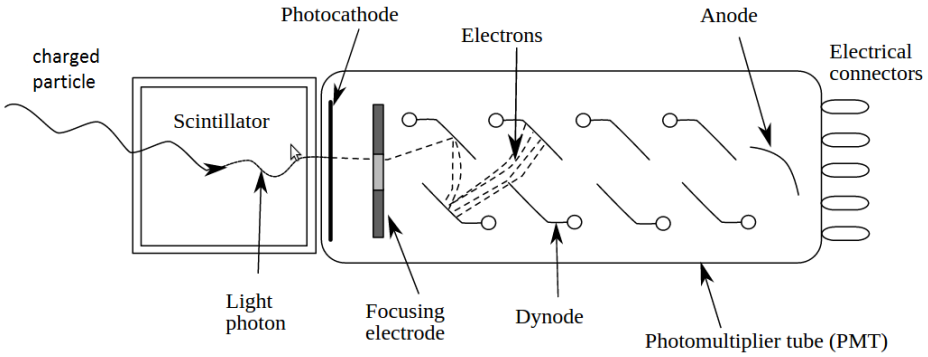

Figure 2.6: Schematic illustration of scintillator and the working principal of a photomultiplier tube [11].

Scintillators are made of materials that produce visible (or near ultraviolet) light, when a charged particle passes through them. The charged particle excites the atoms of the material causing them to emit the light. This light can be amplified if the scintillator is connected to a photomultiplier. In the photomultiplier the photons are converted to electrons via the photoelectric effect. These electrons are focused by the focusing electrode and hit the first dynode where the electrons are multiplied due to secondary emission and sent to the next dynode. This process repeats until the electrons reach the anode and the signal can be read out.

CHAPTER 3

Setup of the experiment

3.1 Setup

As mentioned in chapter 1 STYX is built from old Straw-Tube Tracker (STT) modules of the ZEUS experiment. The modules are simple gaseous detectors as explained in section 2.2. Since the detectors provide information only on the drift times of the passing particle, but do not have internal trigger system, an external trigger system is used. This trigger system is built from two scintillators with photomultipliers attached, placed above and under the modules. The PMT output is connected to a coincidence circuit. The setup of the experiment is shown in figure 3.1. Beside the detector and trigger system electronic devices are needed to convert the data gathered by the detector and send to the computer for further analysis.

Figure 3.1: STYX setup in Bonn with scintillators in black and the modules copper colored triangles.

The heart of the experiment is the modules which are simple drift chambers. Each module has three layers of 88 straws (see figure 3.2). The straws are cylinders filled with a gas mixture of argon and carbon dioxide. The straw is a 50 μm thick copper-beryllium wire surrounded by a conductive tube consisted of a carbon fiber with a thin aluminum layer [12–14]. The radius of the straw tube is 3.75 mm. The length of the straws differ as the module has a triangular form. The shortest straws are 20 cm long and the longest are 102 cm. Each straw is connected to a readout channel in a front-end board. This front-end board contains a preamplifier and a discriminator. For the readout 6 straws are multiplexed together. There are two long front-end (FE) boards with 96 straws connected and one short FE board with only 72 straws. The FE boards send the information to a TDC, time-to-digital converter, and from there the information is processed to a TRB(TDC-Readout-Board). Figure 3.3 shows the connecting scheme of the components [15].

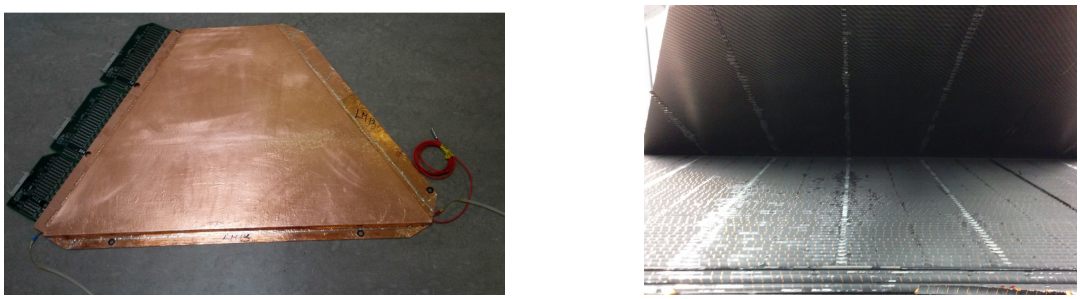

Figure 3.2: A copper colored module of STT (on the left) and straw layers inside one of the modules (on the right).

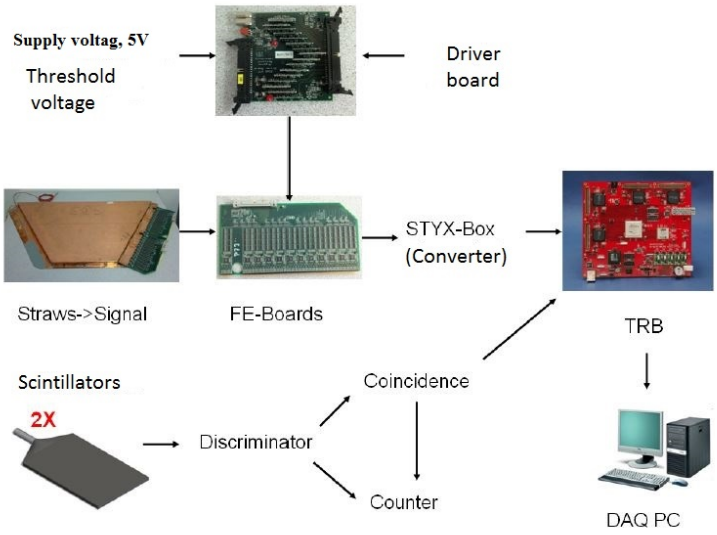

Figure 3.3: Scheme of the STYX experiment. Modules and the trigger system on the left, electronic components (driver boards above, which provide the threshold voltage and are supplying the FE electronics with supply voltage of 5 V, front-end boards for converting the signal (see section 3.3) in the middle, readout board on the right and PC).

In figure 3.4 the connections between FE boards, LVDS (low voltage differential signaling) and driver boards are presented. All the elements are described in the corresponding sections.

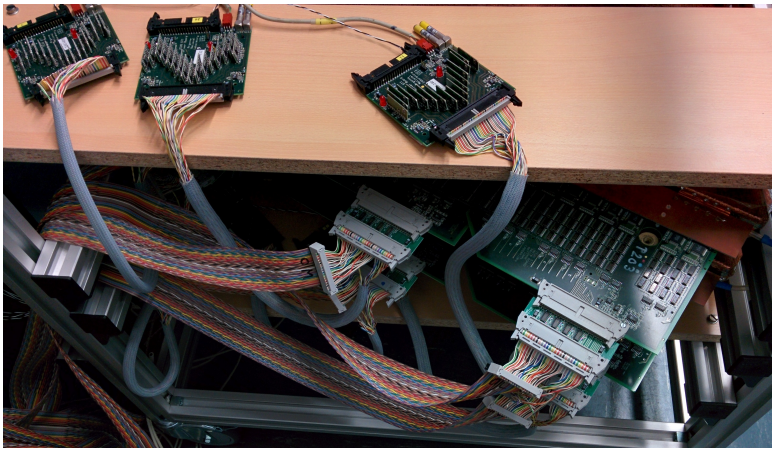

Figure 3.4: Front-end board, LVDS and driver boards connected to each other via ribbon cables.

3.2 Trigger system

As mentioned before, the trigger system is composed of two scintillators attached to photomultipliers and is used to tell the setup that a cosmic ray passed through the detector. PMTs are often used as triggers because they provide a precise time reference. The time resolution of a photomultiplier is under 200 ps, an event has a time window of 200 ns and the expected width of the time distribution is in average 80 ns, but the width differs depending on the gas mixture characteristics. The working principal of a photomultiplier and a scintillator is described in section 2.4. For an event to be registered as such a signal from both scintillators at the same time is expected. Each scintillator is attached via a waveguide to a PMT, which is then connected to a counter. The counters count the number of times, when the signal is above the discriminator threshold. The information from the counters are then passed to a coincidence counter, which then controls if there are any possible events. When the particle passes through the top and the bottom PMT at the same time an event is counted by the coincidence counter and the trigger signal is sent to the readout electronics.

3.3 Readout system

3.3.1 Front-end boards

The analog signal from the straws has to be converted to a digital signal which can be processed by a computer. The signals from 6 straws are multiplexed by a front-end board into one readout channel with a 200 ns delay between each straw. From each straw the signal is converted in three steps. The output of the front-end board is a TTL signal. This is converted to LVDS using an extra board to reduce cross-talk between modules and readout cables. From LVDS boards the signal is processed further to a converter box. At this point, the information about the arrival time is extracted from the digital signal. [12]

3.3.2 TRB - TDC readout board

The HPTDC board (high purpose time-to-digital-converter) was developed at CERN as a general purpose tool for different detectors [16]. The TDC which is used in STYX is included on the HPTDC board and was initially built for HADES-experiment. The TDC is placed on a board, the TDC readout board (TRB). The TRB is easily programmable and can be easily adapted for different experiments. The TRB

has 4 inputs with 32-channels each, the first 31 channels read out the signal and the 32nd channel is used for the trigger signal. The TRB saves all the information that it receives after the trigger signal, which is then delayed and then used again to decide if the information should be stored or deleted. The received signal is then stored on the PC and can be processed further [17].

3.4 Software

The collected data are saved on a hard disk and need to be converted to an event-by-event file which contains drift time information for each straw with a hit in it. For this purpose a software was developed consisting of three main parts: processing the data (M2C2 (Mapping, Merging, Converting, Calibrating), calibration, reconstruction and analysis. M2C2 first converts the data to a .TXT-file, which is then used for calibration. Then the data is reprocessed with M2C2 using the information on the calibration. After that, the reprocessed data can be used for reconstruction and analysis. The single steps will be shortly presented in the following sections and in more detail in chapter 6.

3.4.1 M2C2

The program used to convert the raw data is called M2C2 and it stands for two Ms, meaning merging and mapping of the data, and two Cs for calibrating and converting. The information about the time window and geometry of the detector are saved in the mapping file which is called by M2C2 to process the data in the first step, so that afterwards the written event will have information about position coordinates and the drift times. Already in this step the information from the channels are demultiplexed so that the signal is mapped to the straws from which it was received.

3.4.2 Calibration

The calibration software reads the output of M2C2 where the drift times in straws are stored. Also the straws with no or only few entries cannot be used later in the reconstruction and should be treated accordingly. For the drift time a distribution of 80 ns width is expected, for each channel 200 ns are reserved where this distribution should be found. The distribution for each straw starts at a different time point, so the calibration software determines the offset for each straw and shifts the distribution using this offset, so all the distributions start at the same point, called t_0. The other task of the calibration software is to determine which straws are broken or do not perform correctly. For example, the straws with no or only few hits are marked as dead or the straws in which the distribution is too broad are marked as noisy. The information of the straws from these two cases cannot be used for reconstruction of the events. After the calibration these straws are masked and are not used in following reconstruction and analysis tasks [18].

3.4.3 Reconstruction and analysis

After calibration, the reconstruction of the events can be performed. The first step is to calculate from the stored drift time the drift circles. The drift circle is also called hit later. The reconstructed drift circle are then used to reconstructed the segments, a tangent fitted with a certain tolerance to at least three neighboring drift circles, the hits, coming from each layer in one module in one module and are grouped together.

There are two algorithm used for creating the segments. First needs at least three hits. The algorithm searches for a hit in the middle layer. If a hit is found this straw is then used as a seed straw which means

that the algorithm searches the neighboring straws for hits as well. For example, if the hit is found in the n-th straw of the middle layer, the straws n and n−1 in top and bottom layer are checked for a hit. If the hits are found in this straws a segment can be fitted to this hits.

The second algorithm creates a segment. It works the same way as the first one, starting with the middle layer to look for a seed straw and then checking for further hits in the neighboring straws of the top and bottom layer, but also in the middle layer. For example, the seed straw has the number n, then the straws n−2, n±1 and n are checked for hits in the top and bottom layers and also the straws with numbers n±1 of the middle layer. This way this algorithm checks at least 10 straws for possible hits and uses them to create the segment.

Next step is to reconstruct a track of a particle from the segments. There are again two algorithms for track reconstruction. First algorithm uses two segments, one in each module, to form a track. The algorithm compares the slopes of the segments with each other and if both segments have similar angle a track will be created. The tolerance range for differences of the slopes can be varied. One of the exercises for students is to compare the angles of reconstructed track with the angles of the used segments.

Another way for a track to be reconstructed is to find a segment in one of the modules and a group of hits, later called cluster, in the other. Again a cluster should be found in a tolerance range of the slope of the segment. In figures 3.5 and 3.6 examples of such a segment and of a cluster are presented.

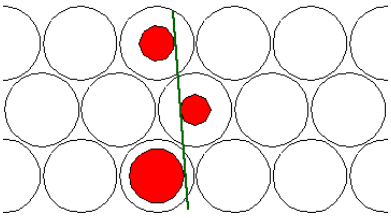

Figure 3.5: Example of a reconstructed segment: three neighbor hits are used to create a segment. Two segments, one in each module can be used to reconstruct a track.

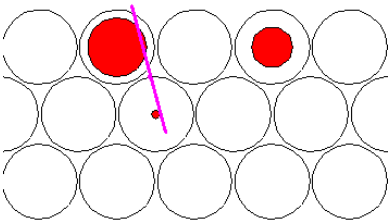

Figure 3.6: Example of a cluster in a module, group of at least two hits in the neighboring straws. The pink line is only used to mark the cluster. The segment can not be fitted using only two hits. A cluster can be used in combination with a segment in an other module to reconstruct a track.

Figure 3.7 contains all the reconstructed elements. The red circles represent the drift circle (hits), the short green lines are the reconstructed segments and the dashed lines are the tracks. The blue dashed line is the track reconstructed using the first algorithm, the pink dashed line was reconstructed using the second algorithm.

With the reconstructed data the analysis can be performed.

3.4.4 Monte Carlo simulation and event display

A Monte Carlo simulation is a tool often used in physics to simulate the behavior of a particle in detector. The simulation starts with creating the tracks in the way that the angular distribution of the tracks has the expected $\cos^2(\theta)$-form and checks afterwards if the distance between track and the straw wire is smaller then the straw radius. If the distance is smaller, it means that the track is passing through this straw and in that case the straw contains a hit. The information about the event (in which module, layer and straw the event occurred and the distance between track and the straw wire, which is the drift radius) is then written to a file.

To make the simulation more visual a software called STYX Event Display is used (SED). SED can simulate any number of events and any number of tracks per event. Each event can then be displayed and worked with. The tabs in SED are: Data, MC, Analysis, Refit and Events. In Data a data file can be uploaded for studies on visual display. MC simulates the given number of events, which can be then individually looked up in Events. In Refit different reconstruction algorithms can be tested. An example of an event in the event display is shown in figure 3.7. Both algorithms of the reconstruction software are presented in this event. The blue dashed line is used in the software for the algorithm which uses two segments in both modules to reconstruct the track, the pink dashed line presents the algorithm which uses one segment in one module and a cluster in the other.

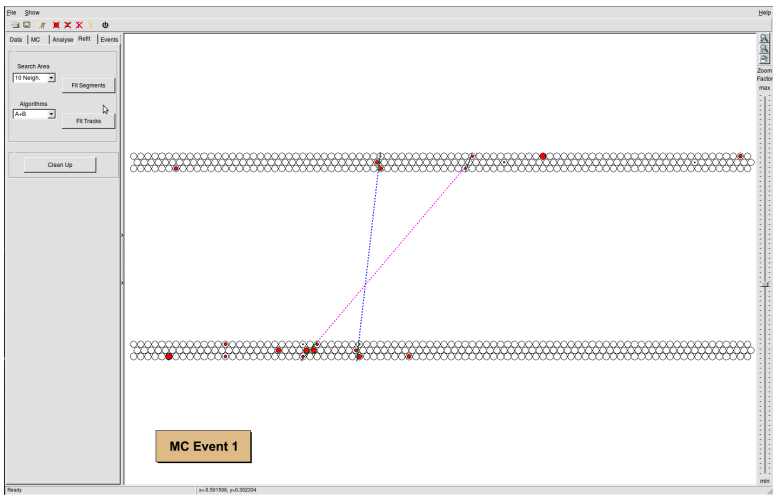

Figure 3.7: An example of an event in SED with two tracks simulated and successfully reconstructed. The blue line is a track reconstructed using two segments in both modules. The pink line is a reconstructed track using the second algorithm, one segment and one cluster. Red circles are drift circles calculated from the drift radius.

CHAPTER 4

First studies of the experiment

4.1 Introduction to the experiment

The best way to look for the possible improvements of the experiment is to perform the experiment. STYX is one of the experiments in the laboratory course of the University of Bonn which gives a good opportunity to study it. The work started with performing the experiment as if a participant of the lab. course of the university would carry it out.

Before starting to take data the components of the experiment have to be prepared. The working voltages for PMTs are determined and the threshold voltage of the front-end electronics is chosen. The voltages for PMTs are changed in a range from 1700 V to 2300 V in steps of 50 V and the notes on counting rate are taken. For each voltage at least three numbers should be registered to avoid systematic errors. Then arithmetic mean and standard deviations are calculated and plotted. The numbers are presented in table A.1 and in figure 4.1 for upper photomultiplier. First, an exponential rise can be seen as expected. This effect occurs due to rising number of detected muons. After a point where all muons are detected a linear rise occurs. There are no more muons to be detected and further increase of the voltage only amplifies the noise. Correspondent functions were fitted to the data points. Based on observed intersection point of both functions the working point was set to 2100 V.

Then the voltage for the bottom PMT is varied in the same range. Now the counting rate of the coincidence is registered. The arithmetic mean and standard deviation are calculated and represented in table A.2 and in figure 4.2. First, a linear raise is expected following by a plateau. The functions were again fitted to the points and it was decided for working point to be set to 2050 V.

Next threshold voltage of front-end electronics need to be determined. The purpose of this threshold is to reduce electronic noise but at the same time not to lose too many events. Different voltages, 1.4 V, 1.8 V, 2.0 V, 2.4 V and 3.0 V, were tested. The comparison of the effect of the threshold on drift time distribution for one of the channels in TDC1 is presented in figure 4.3. Based only on this plot the decision about threshold voltage cannot be done. The rate of counted events should also be compared so that not too much signal would be lost. The Rate for the same channel in same TDC can be found in figure 4.4. After comparing the rate for different threshold voltages and taking into account how much noise was reduced it was decided to set working point to 2.4 V.

After setting up the threshold, a large amount of data can be taken overnight to gather enough information for calibration and analysis. After the calibration is performed with a small amount of the overnight data it can be applied to the remaining data which is then used for analysis and reconstruction.

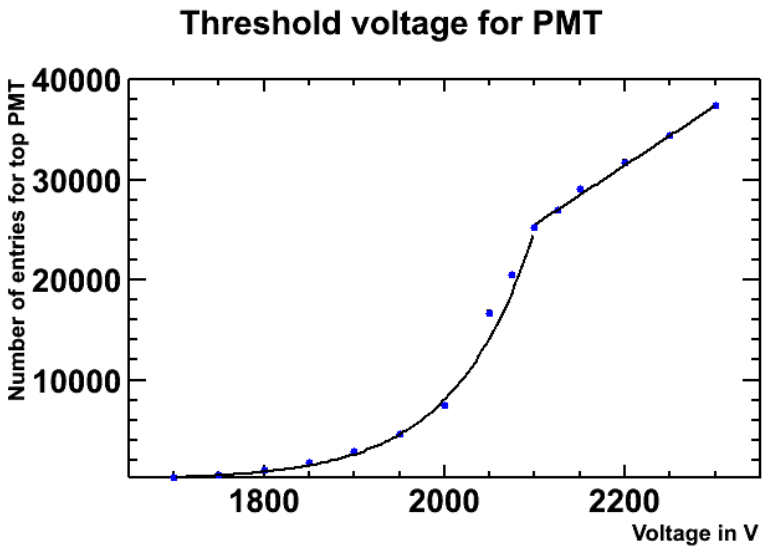

Figure 4.1: Determination of threshold voltage of the top photomultiplier

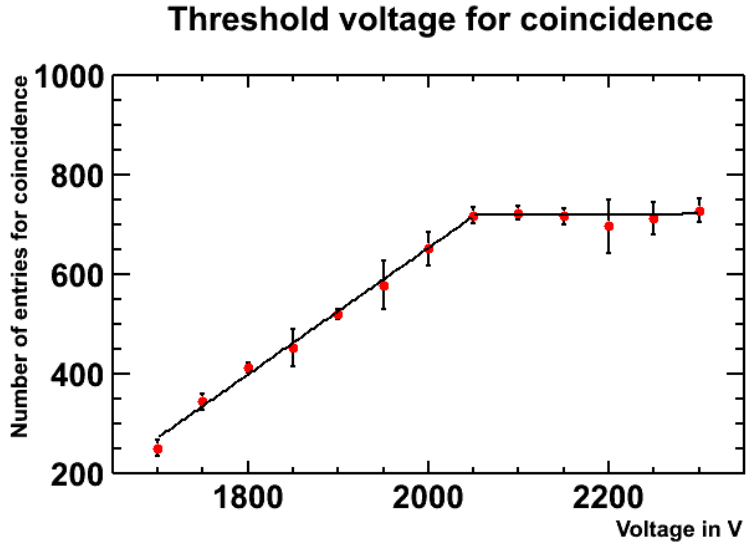

Figure 4.2: Determination of threshold voltage of the bottom photomultiplier.

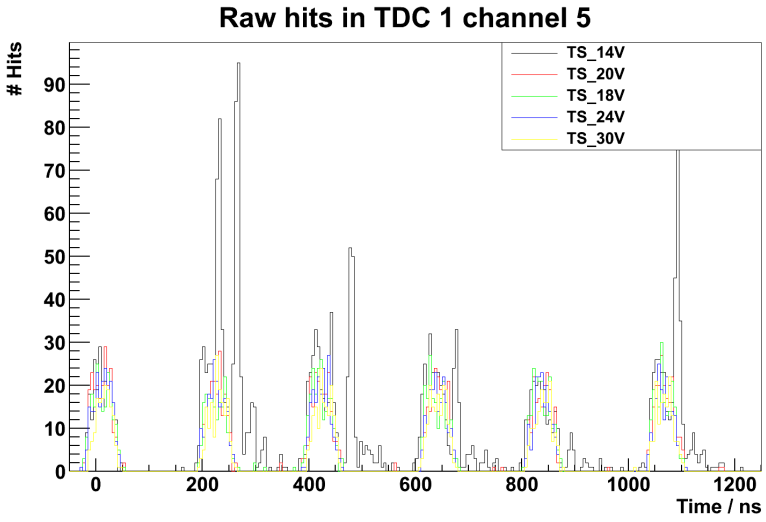

Figure 4.3: Comparison of different threshold voltages of front-end electronics for TDC 1, channel 5

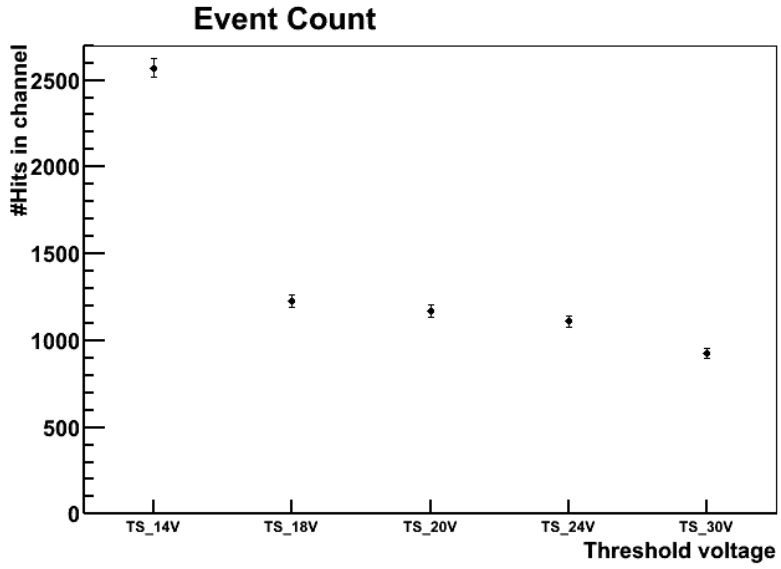

Figure 4.4: Comparison of counting rate for different threshold voltages in TDC 1, channel 5

All of the steps are done in the laboratory, next to the experiment. In the time while waiting for the reconstruction to finish, the hardware, the setup and the development step of the experiment can be studied.

After the experiment is finished and the data is processed, the results are studied to discuss possible points where the improvements are needed. To understand the working process further explanation of the software is presented in the following sections.

4.1.1 Calibration

Calibration is the first step after the raw data was converted. In this step it is decided if the straw can be used in further studies. There are four states of the straws: good or working straws, dead, continuous and noisy, the examples of the distributions are shown in figures 4.5 - 4.7. In figure 4.8 each straw of the modules is shown in colors defining the status of this straw. The good or working straws show the expected drift time distribution. Noisy straws are the straws with too many events in a straw, there is almost always a hit in these straws, which means there are hits registered in such straws, even if there was no actual particle passing through the straw. On the other hand, dead straws do not have any hits in them at all or very few, so that the drift time distribution is empty or almost empty. Continuous straws are the straws which aren't dead or noisy, but still cannot be calibrated with the calibration software. For example, if the drift time distribution in a straw is too narrow or too broad, such a straw will be marked as continuous. If six straws are showing the same errors, all are dead or noisy, the suspicion is that the problem may lie not in the straws but in the channel or rather in the electronics.

The calibration is called straw-by-straw calibration or t_0 calibration because the calibration is done for each straw and searching for an offset, t_0 where the drift time distribution is starting and the noise ends. The main calibration tool is finding the starting and ending points of the distribution and then deciding the level of the background noise. The events with a number of entries less then noise are then treated as noise and everything else as the signal. The width of the drift time distribution should not be less then 50 ns or more then 120 ns otherwise the straw is marked as continuous, as the time distribution of a good straw (see figure 4.5) has usually a width of $\approx$80 ns. There are also other, secondary, calibrations which are used for cases when the main calibration is not enough. A more detailed explanation on calibration can be found in the bachelor thesis written by Dustin Hebecker [18]. A visual example of the quality of the calibration is shown in the figures 4.9 and 4.10 for the third layer of the second module, with the drift times plotted versus the straw number. The distributions are shifted correctly to 0 ns and the problematic straws are masked with a few exceptions.

4.1.2 Reconstruction

After calibration is finished, reconstruction and analysis have to be performed. The information about drift time is gathered from the data file and used to calculate the drift distance. As it cannot be know exactly where the particle crossed the straw a circle with this drift distance as a circle is drawn around the wire. At least three such circles are needed to create a segment. The software searches the middle layer of the first module and if a hit is found it scans the neighboring straws in the other layers to find at least two more hits. If no more hits are found, the hit in the middle layer is probably just a noise hit and is discarded and the search continues. If there are hits found and a segment is created, reconstruction software searches for a segment in the other module with similar slope and tries to create a track. The track slope can differ from the segment slope a little. The track connects two segments in both modules. The slope of the track is therefore a combination of slopes of the segments.

In Monte Carlo simulation the tracks, one or more, are simulated in a way, that a $\cos^2(\theta)$-form of the

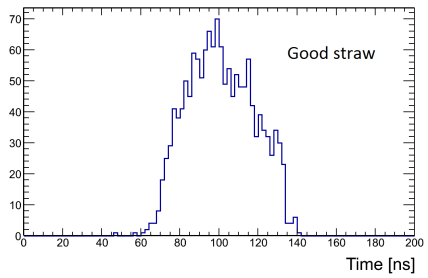

Figure 4.5: Drift time distribution of a good straw. On the *Y*-axis number of entries and on the *X*-axis the drift time are plotted.

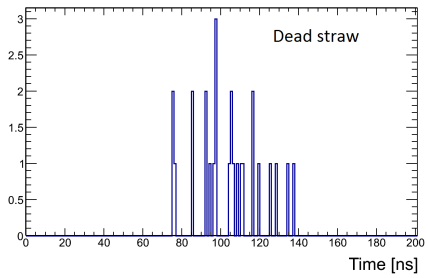

Figure 4.6: Drift time distribution of a dead straw. On the *Y*-axis number of entries and on the *X*-axis the drift time are plotted.

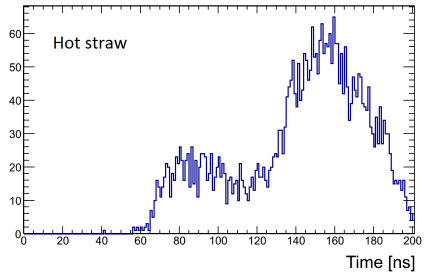

Figure 4.7: Drift time distribution of a hot straw. On the *Y*-axis number of entries and on the *X*-axis the drift time are plotted.

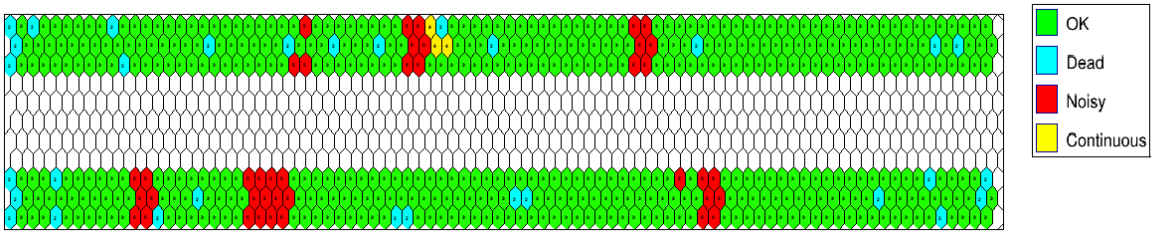

Figure 4.8: Straw mask of the modules: colored combs are straws which form three layers of the both modules.

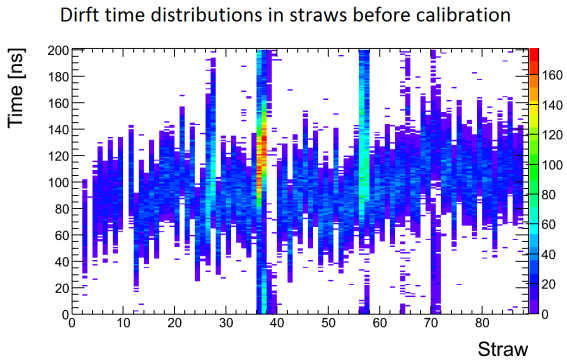

Figure 4.9: Drift time distribution before calibration for the third layer of the top module.

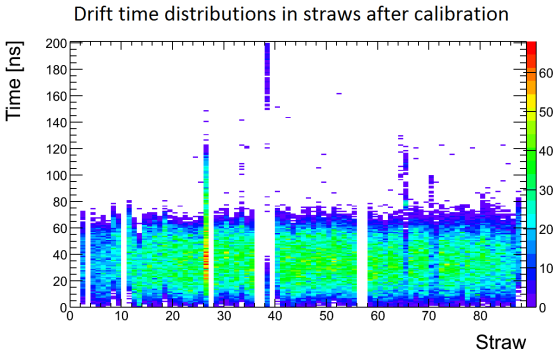

Figure 4.10: Drift time distribution after calibration for the third layer of the top module.

distribution is achieved. In contrast to the data the drift distance of the track to wire is stored and not the drift time. Otherwise reconstruction works in same way with the drift time calculated from the distance.

A linear dependence is assumed of the form:

$$r_{drift} = (t_{drift}/80) \cdot t_{straw} \tag{4.1}$$

with:

- r_{drift}: drift distance of the electrons in mm
- t_{drift}: drift time of the electrons in ns
- r_{straw}: radius of a straw, which is a constant value, $r_{straw} = 7.495/2$ mm

For the simulation the equation is changed so that the drift time is calculated from the distance.

After the reconstruction is done, the information about each event are stored in C++-objects. For example, the SHit class contains all the information on the hits in the events, or STrack the information about reconstructed tracks. With this information the analysis can be performed.

4.1.3 Analysis

The analysis uses the objects stored during reconstruction to create the histograms that can be examined later. There are many variables that are interesting to study. From the particle physics point of view the drift time distribution and the angular distribution of the muons are the most important. From the point of view for the possible improvements or studies of the hardware the display of the modules with good or bad straws as well as distributions of events in the modules are convenient.

In figures 4.11- 4.12 the angular distributions of segment and track slopes for data (black line) and simulation (red line) are presented. The distributions definitely are not of the $\cos^2(\theta)$-form. There seems to be a preferred angle around 0.55 and 0, it is more likely that a segment is reconstructed at this angle. But there are also some segments "missing" at the other angles. For segments this phenomenon is more pronounced than for tracks. That can be explained due to the use of two different algorithms, if the first algorithm did not found a track with a segment, the second algorithm can probably match a cluster to this segment, and so compensate the "missing" angle in the distribution. In the same distribution

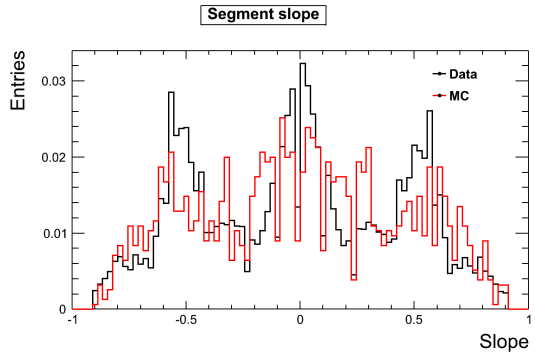

Figure 4.11: Overlay for data (black line) and MC simulation (red line) of distribution of segment slope.

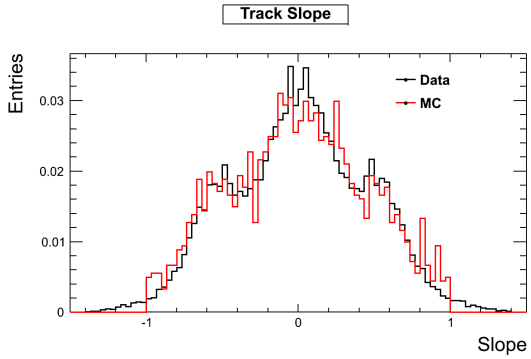

Figure 4.12: Overlay for data (black line) and MC simulation (red line) of distribution of track slope.

for the simulation the peaks are at the same position as in data histograms, but less pronounced. Also the distribution for the tracks is more narrow. It seems that the simulation does not describe the data correctly. The form of the distribution still does not correspond to the expected $\cos^2(\theta)$-form, which shows that the improvements of the reconstruction software are needed.

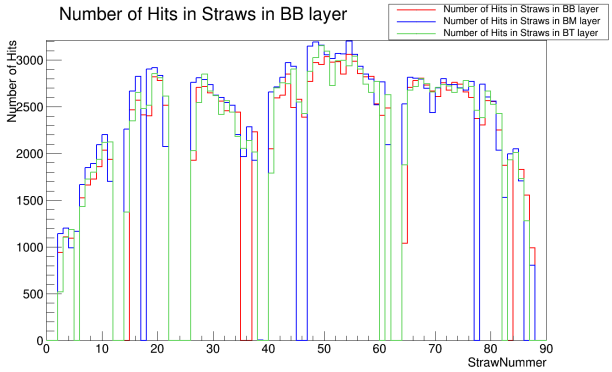

Figure 4.13: Number of hits vs the straw number in cosmic data for the first module and all three layers.

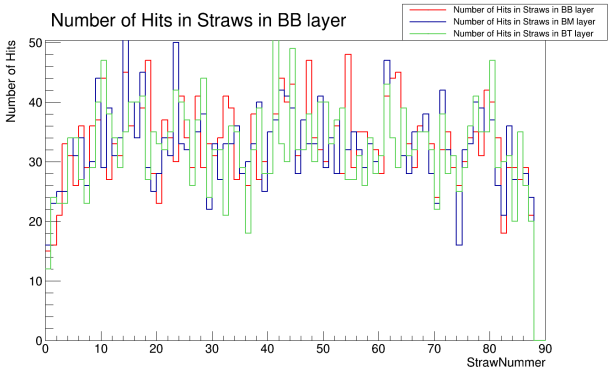

Figure 4.14: Number of hits vs the straw number in Monte Carlo simulation for the first module and all three layers.

The same problem but also one possible solution can be seen in figures 4.13 - 4.16. These show the numbers of hits versus the straw numbers for all three layers in both modules. After the calibration the signals of a few straws are not considered or are masked. In the histograms these straws do not have any hits in the end and are missed in the reconstruction. It means if a charged particle passed one such straw the possibility to reconstruct this event is smaller. The simulation does not consider the possibility of the "dead" or non-working straws. In addition the distribution in general looks smoother for the simulation due to the geometry of the scintillator, which is not implemented in the simulation.

In figure 4.17 the setup of the experiment is shown. The scintillators used in Bonn do not have the same form as the modules, which means some events are lost, if the particle would pass through the module without passing through the scintillators. The simulation assumes the same probability of

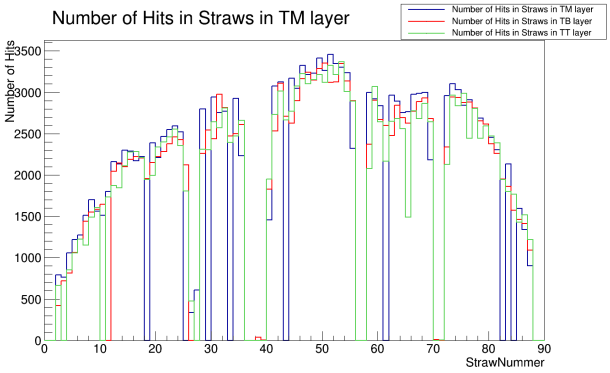

Figure 4.15: Number of hits vs the straw number in cosmic data for the second module and all three layers.

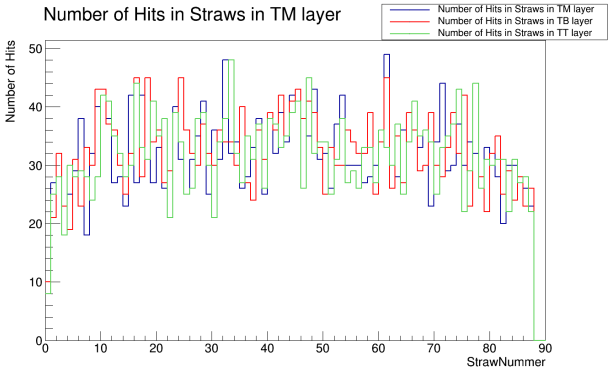

Figure 4.16: Number of hits vs the straw number in Monte Carlo simulation for the second module and all three layers.

Figure 4.17: Schematic setup of the experiment with two modules (copper colored triangles) and two scintillators (black rectangle) with attached PMT (metallic tubes) as the trigger system.

detecting a particle for all straws without considering the straw length and position. In the short straws fewer events are expected. In the data only information about two of three coordinates are stored, in which straw, the horizontal position, and in which layer and module, the vertical position of event in experiment, but it is not possible to say where exactly in the straw the particle passed through. It means the simulation simulates an event equally for all the straws. In data, however, events are lost if particle is passing through module, but not through scintillators.

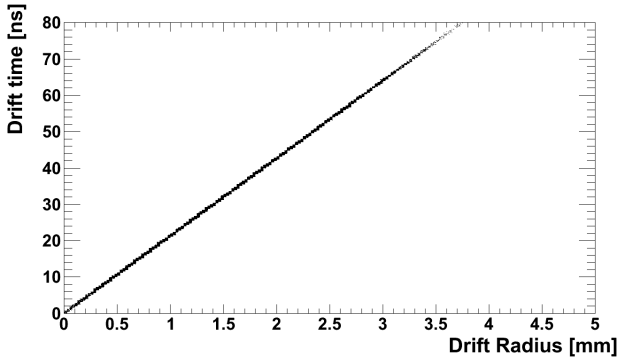

Figure 4.18: Linear dependence of the drift time from radius for data.

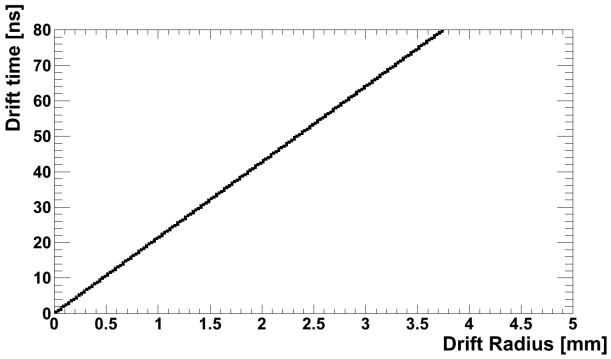

Figure 4.19: Linear dependence of the drift time from radius for simulation.

Another aspect, where the simulation does not describe data properly, can be seen in histograms. For example, in figures 4.18 and 4.19 the dependence of the drift radius on the drift time is shown for data (again on the left side) and for simulation (on the right). As mentioned above, the linear dependence is assumed which can clearly be seen in the histograms. But data has fewer events for smaller radii as well as for the larger radii. Again, Monte Carlo simulation does not consider the losses due to the detector geometry. Besides, as in the simulation the drift radius is simulated and not the drift time, and the possibility to be simulated is the same for all radii .

4.2 Identified problems and plans for improvement

From what has been said before there are a few areas where the improvements of the experiment can be performed. The working blocks can be divided into two areas: improvements that can be performed with the software and improvements or, better to say, possible fields to studies of the hardware.

The software is rather extensive and has to be studied more carefully before the improvements can be developed. There are however a few things that can be mentioned already. First of all the segment based reconstruction of the event should be improved. It is slow and, sometimes, the segment reconstructed with wrong angle, which makes reconstruction of the tracks difficult. Still, the reconstruction of the tracks can be improved so that the angular distribution is more smooth.

The simulation is also a part of the software. The possible improvements for the simulation are making it describe data more closely. It can be achieved if the geometry and the defects of the detector are implemented.

Those are only first ideas of the possible improvements. After further studies of the software can bring new ideas.

The studies of the hardware can be performed on many stages: electronics, the modules and cables. All the elements have to be tested individually and then together. At the electronic stage it can be tested and decided, why the straw or a whole channel is not working and, if possible, to resolve the problem.

CHAPTER 5

Hardware developments

From chapter 4 it can be concluded that improvements are necessary for the following points: test of electronics and hardware parts such as cables and connections between chips. Testing of the modules is also planned and should be performed not only for the installed modules but also for the modules stored in the store house. For this purpose a setup similar to the one developed at ZEUS for testing of the modules after transportation was implemented. The main part is a switch box to which the cable from the front-end boards can be connected and each channel can be switched on or off separately. In figure 3.4 in chapter 3 the connections between electronic parts are shown. The switch box is on the end of the ribbon cable. There is a threshold voltage applied to the driver board via the thin black and white cable and is supplied with power via the cable next to it.

5.1 Test pulses

5.1.1 Switch-box

The switch-box was built for the test of the modules at ZEUS, DESY. The box just enables the connection of the ribbon cables from the front-end board to an oscilloscope. There are 16 channels in each front-end board, so there are also 16 switches on the front board of the box. These switches allow to switch on each channel separately from others. There are two rows of 8 switches, each row is connected to the one of two lemo sockets in the other side of the box. Each socket processes the signal from 8 channels of the front-end board. The switch box can be seen in figure 5.1.

5.1.2 Hardware test

To test the hardware a test pulse was generated. For this purpose a pulse generator was added to the setup. The signal is first generated in the pulse generator and then send to a driver board. Te driver board is then generates a test pulse every time, when the negative flank of the signal from the generator arrives.

The signal is first found on the oscilloscope to confirm the form and length. Then the pulse sent to the electronics of the experiment, driver boards, and then to the oscilloscope via the ribbon cable. The output signal is from one channel which means it is displaying six peaks for six straws of the channel. An example is shown in the figure 5.2 for the setup in Bonn. All the straws are displayed evenly. The signal is transmitted by a twisted-pair cable, one for the signal the other is for the inverted signal. On

Figure 5.1: Test pulse setup used for testing hardware of the experiment. The ribbon cable from FE boards is connected to the switch box. From the switch box the signal is displayed on the oscilloscope.

the oscilloscope's monitor are three lines, two are the signal (in blue and yellow) and the third one is the sum of the signal.

Figure 5.2: Test pulses in a working channel at STYX at Bonn. Blue and yellow lines are the signal from the ribbon cable, red line is the addition of both, blue and yellow, lines.

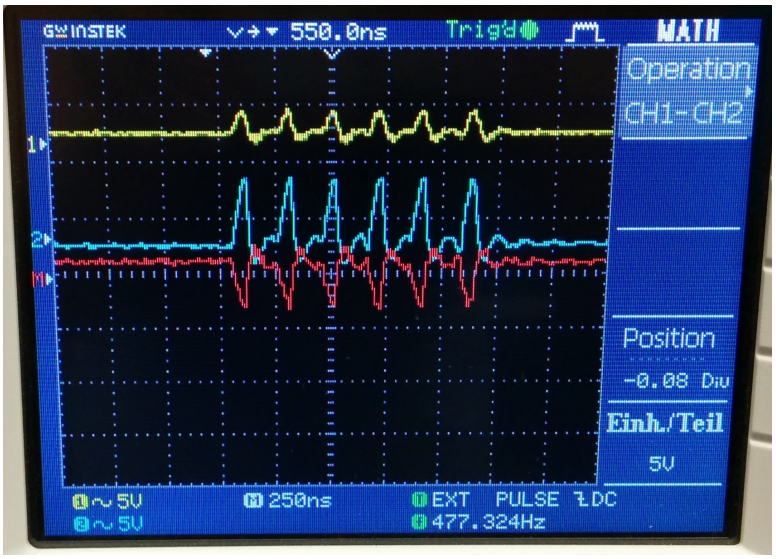

Figure 5.3: Test pulses in a problematic channel at STYX in Bonn. Blue and yellow lines are the signal from the ribbon cable, red line is the addition of both, blue and yellow, lines. The signal from one of two channels (yellow line) is deranged and the blue line shows extra peaks.

In figure 5.3 is an example of the "broken", not properly working, channel. In comparison to the signal in the first figure the height of the signal here is lower and between the peaks the noise is showing. The cause of the problems in this channel could be a defect cable, because the signal is still coming through, but the signal is misshaped. Also the additional peaks are an indication for the cross talk between the

two neighboring cables of one straw in the ribbon cable.

The systematic tests of the hardware started with a test of the stored modules. The switch box was connected to a driver board and one of the front-end boards, which was not joined with any module to test the setup first. Then the pulse generator was plugged into the driver board via the input next to the power supply of the driver board (see figure 3.4 in chapter 3). This signal inputs a pulse to the input of the ASDQ that then processes this pulse as if it were a signal coming from the wire of the straw. That signal would be usually sent to the readout electronics. Using the same setup, the signal is redirected with the same ribbon cable to the switch box and then to an oscilloscope, where the signal can be displayed. With this method a few different front-end boards and with different driver boards were tested. This way it was possible to make sure that the cable used for the test was not broken or showing any damage. If in the different front-end boards and driver boards the similar problem occurred for the same straw, it would indicate a problem with the cable. For example, if there is a cross-talk between the neighboring cables of the ribbon cable, the same straws in different FE boards would show a second peak in the signal or misshaped signal. The cables with such problems were replaced.

However, a strange behavior of the front-end boards was seen. If a front-end board showed a broken straw or channel itself in one of the rows of the box the same straw or channel appeared to be broken in the other row as well. After a few tests it was concluded that the cables were connected wrongly in the switch-box. After the switch-box was fixed the test of the modules had to be repeated. The information on the status of the modules will be stored in the data bank of the experiment.

Figure A.2 shows one of the working channel from the setup at CERN. Figure A.1 presents one of the broken channels. As part of this thesis, a trip to CERN was organized to resume the experiment. At CERN everything had to be connected from the beginning. The test-pulse setup was taken along to perform the tests there as well. During the test it was realized that the test setup could be used to improve the calibration. The improvements of the calibration are described in a bachelor thesis [19] and are summarized in the section 5.1.3.

5.1.3 Calibration with test pulses

Beside the testing function the test pulses can be used to perform the calibration of the electronics, even before the data was taken. The test pulses are set up as explained above except that here all the six front-end boards had to be connected at the same time. As the generator only has one NIM-output a fan-out has to be used. The fan-out takes the output of the generator as an input and creates four more outputs. These outputs can be used again as the signal for the front-end boards or trigger system or as the output signal for the next fan-out input. This way all the front-end boards receive the same signal, but with a delay, which can be seen in the time distributions. The fan-out is put between the generator and the trigger electronics. The signal is distributed between the front-end boards and the trigger signal which is sent via a trigger-signal box to the TRB.

The test pulse is treated as data. After the information are stored, it should be converted with M2C2 and then calibrated with calibration software. This is done in two steps. First the information about the pulses is written to a raw file. For each straw the distribution of the pulses is much narrower then the drift time distribution for cosmic data. Therefore, every straw has a narrow peak at a defined position in the time window depending on which straw in the channel it is. For each straw the peak position is found and then the peaks are moved to a set point. This set point can be chosen freely first. The information on the difference between the set point and the peak position is stored in a file and can be used for calibration of the cosmic data as well. The interesting point is to see if the test pulse calibration improves the calibration from before, makes it more precise or if it runs faster. Besides, the test pulse calibration also marks the straws as pulse dead or noisy, as well as pulse calibrated. It allows one to

identify if the problem is the electronics, which is broken, or if there is a problem with the straw itself.

In figure 5.4 the straw mask after calibration with the test pulses is shown. Only a few of the straws are dead. The status of the first two straws in each layer of the both modules is set to ”dead” automatically and the calibration starts from the third straw. In figure 5.4 only the first straw is marked as dead. The number of straws in this mask is also only 87, and not 88. It indicates, that there is a problem in the software, which causes that first straw is not added to the straw mask. It is fixed in the later straw masks. There are also not too many noisy straws. So it can be said, that the electronics of the two modules are working properly.

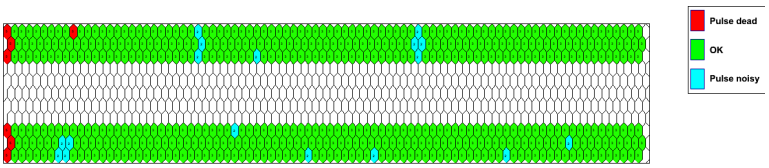

Figure 5.4: Straw mask for data calibrated with test pulses.

After the pulse calibration is performed, the information of this calibration can be used to perform the t_0-calibration. The time distribution of each straw is then moved by the value calculated for the test pulses as explained above. At this point it is important, that the set point is chosen carefully so that the distributions are not moved too much. The time distributions are concentrated in the time window of 200 ns. If the set point for the test pulse is set too low, the drift time distribution is moved to the negative times and out of the time window, or, if the set point is too high, the time distribution is moved above the edge of 200 ns. In both cases the calibration for such distributions cannot be performed, because the start or end point of the distribution cannot be determined and the straw is then marked as ”continuous”. After a few tests, the set point was set to 100 ns. The time distributions for each straw after the both calibration were performed are shown in example histograms in figures 5.5 and 5.6 and in appendix A.3 - A.6.

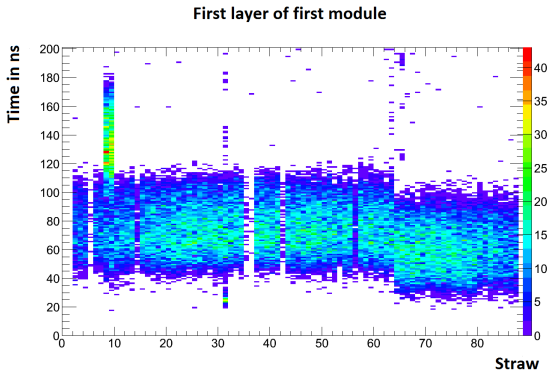

Figure 5.5: Calibration with test pulses for bottom module, first layer. On the Y-axis drift time in ns and on the X-axis the straw number are plotted.

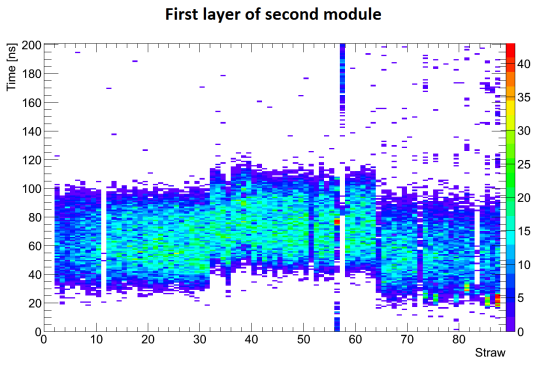

Figure 5.6: Calibration with test pulses for top module, first layer. On the Y-axis drift time in ns and on the X-axis the straw number are plotted.

In figure 5.7 the straw mask after both calibrations is shown. There are more straws which are marked as dead and noisy. The straw’s status from the pulse calibration is also presented. The dead straws now can be explained as the straws are somehow disconnected from the electronics or even broken and the noisy straws indicate the problems with the gas flow inside of one particular straw. These problems are

difficult to deal with.

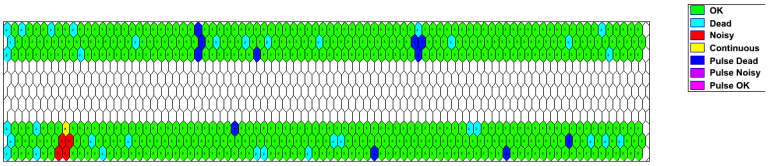

Figure 5.7: Straw mask after calibration with test pulses. The colors for ”dead” and ”hot” statuses are different in this mask. It will be changed for later plots.

5.2 Implementation of the test pulses and results

The test pulses are used to calibrate the straws before the t_0-calibration. The difference between the peak position of the distribution in one straw and the set point is subtracted from the each point in of the drift time distribution of the data. The distributions of all straws of one layer after the shift are shown in figure 5.5 and 5.6. There are steps in the distributions which are concluded to come from the different FE boards. It was decided to test if the calibration FE board by FE board is possible and it would contribute to the improvements of the experiment. This calibration was tested for the setup with three modules. The results are presented in section 5.3.3.

5.3 Assembling of the third module

To find a way to improve the experiment even further more information about the efficiency of the detector was needed. It was decided to add one more module to the setup, in order to be able to measure the efficiency of the straws independent of the tracking. With a third module, it is also possible to investigate the alignment of the modules with respect to each other.

This study has, however, not yet been performed. There were many unused old STT modules, which first were tested with the test pulses to determine if the electronics are still working. The module with the least problems was chosen and placed in the experiment.

5.3.1 Gas and cable connections of the third module

The third module is placed between the two other modules and has to be connected to the gas and the electronics system of the experiment. The gas system is used at the same time with the other experiment in the same room and could not be adjusted easily. The third module therefore has to use the gas tubes that are already there. The gas flows from bottom module to the top module and leaves the room through the small opening in the window. The third module is then connected to the bottom module and leads the gas to the top module. The gas system has to be glued carefully, so that no gas escapes to the room. If the system is not leak proof, the top module may show problems as the gas would not fill it properly. As the third module is placed between the two others it will be referred to as the middle module, so it won't be confused with the top module, which is now the actual third module. Since the modules were stored in the storage for some time before the middle module can be used for data taking it should be flushed with the Ar/CO_2 mixture. For this purpose the gas has to stay turned on for a few days before the data can be taken.

Beside the gas tubes, the electronic cables also have to be connected, but first prepared and tested. After a few attempts the cables were ready and connected to the driver boards as well as to the FE boards. From there the cables go to the converter box, which is the last step before the TRB. The task of the converter box is to gather the information from two ribbon cables from a FE board and convert it so it can be read out with only one flat cable. The converter box has 8 slots, six of them are already occupied with the six cables from the FE boards of the top and bottom modules. The two remaining slots are then used for the two long FE boards of the middle module. Also the TRB only has four slots, three of them are used for the two modules already, the last one is now connected to the middle module.

After the middle module is assembled and gas flushed, the data taking can be started and the usual procedure can be performed. The data is converted with M2C2 and the calibration is applied. The resulting straw mask of all three modules is shown in figure 5.8. The short FE board of the middle module is not connected, therefore all the straws have the status ”dead” in the mask, otherwise the module seem works well.

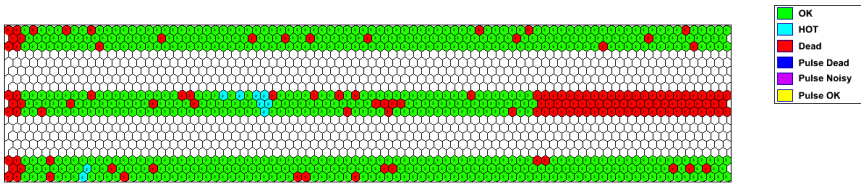

Figure 5.8: Third module: Straw mask for all three modules.

For the software to work with three modules instead of two, a few modifications of the code have to be performed. These will be discussed in the next chapter about the refactoring and software modifications chapter 6.

5.3.2 Calibration with three modules

With the new setup, the working process of the test pulses and t_0-calibration have to be adapted and tested again. In figures 5.9 - 5.14 drift time distributions before (left column) and after (right column) t_0-calibration are presented. Test pulses are not applied yet. It can be seen really well in the distribution before the t_0-calibration. The drift time distributions of each straw in the left plot start from a different point. After applying the test pulses the straws are expected to have the same or at least similar starting point of the drift time distribution as the test pulses are applied on the electronic level of the calibration and just moving the whole distribution by specific value.

While implementing the test pulse into the calibration software a problem with converting of the test pulse data was detected. After converting the data and performing the calibration in the straw mask for the test pulses data in the first layer of every module every second straw was marked as "dead", figure 5.16. This happens if one of the straws in a channel cannot be read out, which could mean that the channel is broken or information from one straw is lost while converting raw data. The time distributions for each channel can be controlled after the conversion is performed. One example of such plot is shown in figures 5.15. It looks like the pulse was stored for all the straws, though compared to data the first pulse is registered ≈ 200 ns later, hence it was cut and is not used later. The reason is that in the mapping file the time windows where the drift time distributions are expected to be found is set so that the cosmic data can be easily converted. That means that if the test pulses are coming at 200 ns, which defines the time window reserved for one straw, then there is no information that can be found in the first window. It also means that information from the last pulses are cut as there is no reserved time

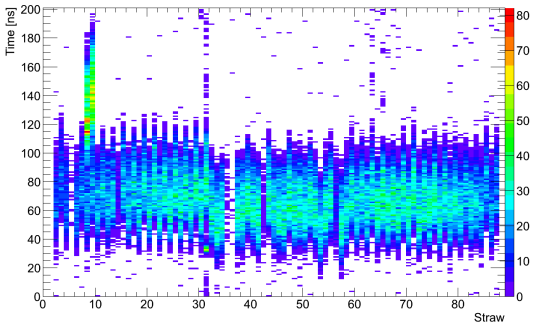

Figure 5.9: Uncalibrated with test pulses for first module, first layer. On the Y-axis drift time in ns and on the X-axis the straw number are plotted.

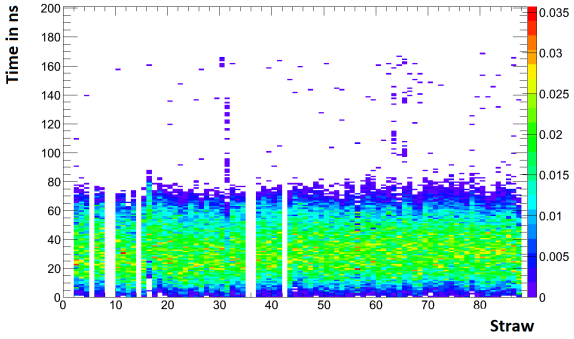

Figure 5.10: Calibrated for bottom module, first layer without test pulses. On the Y-axis drift time in ns and on the X-axis the straw number are plotted.

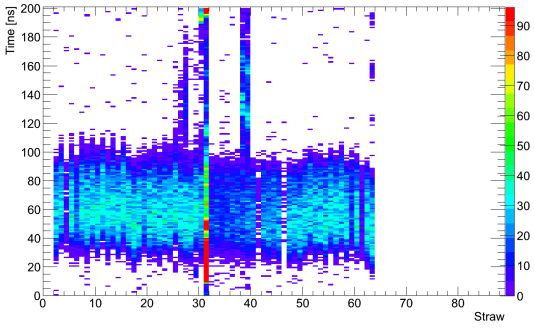

Figure 5.11: Uncalibrated middle module, first layer without the test pulse calibration. On the Y-axis drift time in ns and on the X-axis the straw number are plotted.

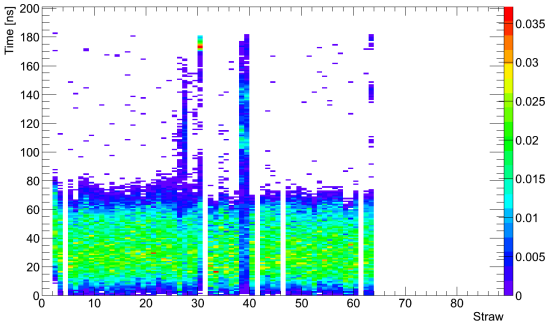

Figure 5.12: Calibrated for middle module, first layer without test pulses. On the Y-axis drift time in ns and on the X-axis the straw number are plotted.

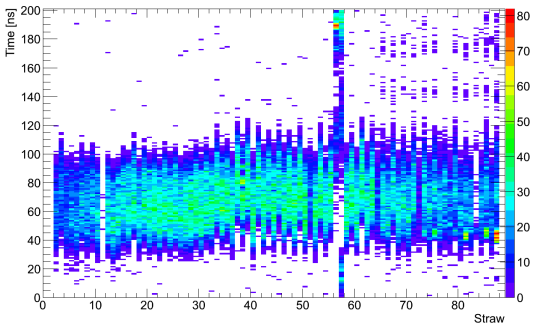

Figure 5.13: Uncalibrated for top module, first layer without test pulses. On the Y-axis drift time in ns and on the X-axis the straw number are plotted.

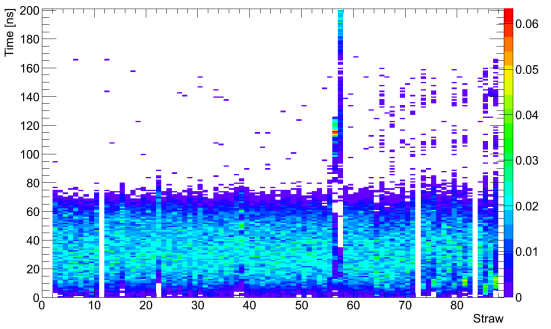

Figure 5.14: Calibrated for top module, first layer without test pulses. On the Y-axis drift time in ns and on the X-axis the straw number are plotted.

window above 1200 ns. It leaves only five test pulses in each channel instead of six.

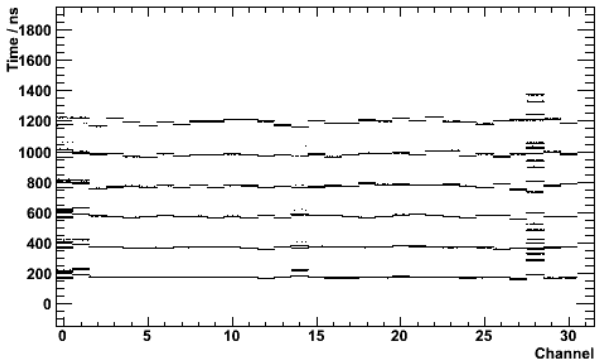

Figure 5.15: Time peaks distribution for TDC, one of the readout channels of TRB. The lines are the starting point of data registration in the TDC. On the *X*-axis the channels and on the *Y*-axis the different starting times are plotted. The 28th channel is noisy.

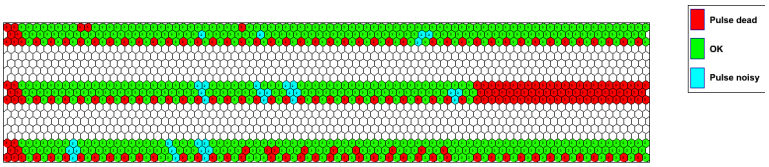

Figure 5.16: Third module: Straw mask for all three modules for test pulses.

In the previous chapter this problem was dealt with using two different mapping files for the test pulses and cosmic data with different time windows. But as it is wanted to use the test pulses in the lab. course later this way of solving the problem with different time windows is inconvenient. Another possibility is to use a delay for the test pulses, so that the test pulses would have the same starting point as the data. For this purpose a delay box and two cables with delay value of 100 ns each were added to the setup. As the time window for one straw is 200 ns it is not necessary to delay the test pulses more than by this value.

First a delay of only 60 ns was added. After converting and calibration were performed the straw mask for the test pulses shows the same problem as before, each second straw in the first layers of each module are marked as "dead" and cannot be used. As a result too many events cannot be reconstructed. In the figure 5.16 this straw mask is presented. Figures 5.17 - 5.19 the problematic layers are shown. The histograms of the other layers can be found in the appendix, in figures A.3 - A.6.

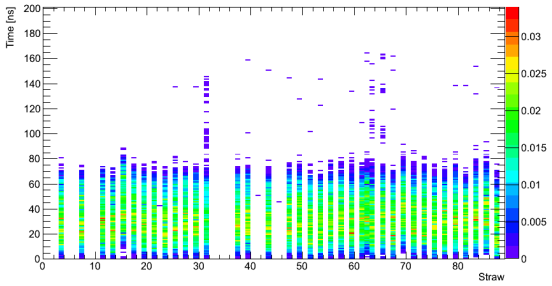

Figure 5.17: Calibration with test pulses for bottom module, first layer for a delayed by 60 ns.

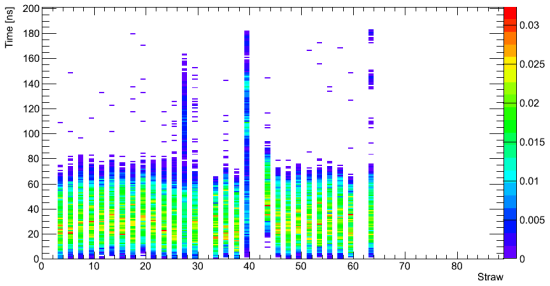

Figure 5.18: Calibration with test pulses for middle module, first layer for a delayed by 60 ns.

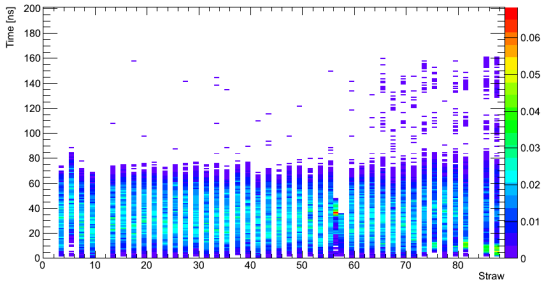

Figure 5.19: Calibration with test pulses for top module, first layer for a delayed by 60 ns.

The same procedure was performed for delays of 160 ns and 200 ns. In figures 5.20 and 5.21 the monitoring files of the time windows for the pulses delayed by 160 ns and 200 ns, respectively, are shown. In the mapping file the time windows are starting from −50 ns and go until 1150 ns in steps of 200 ns. In the monitoring histogram for 160 ns delay the last line lies at the edge of the last time window. For 200 ns the line is shifted further, so that the signal is in readout time window, hence it seems more suitable for the future use. The histograms containing the drift time distribution of the layers in modules are presented in figures 5.22 - 5.27 for the first layers of each module and the others can be found in the appendix, figures A.13 - A.18 and figures A.19 - A.24.

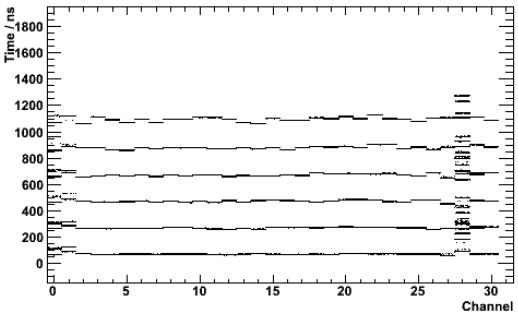

Figure 5.20: Third module: Time peaks distribution for TDC delayed by 160 ns.

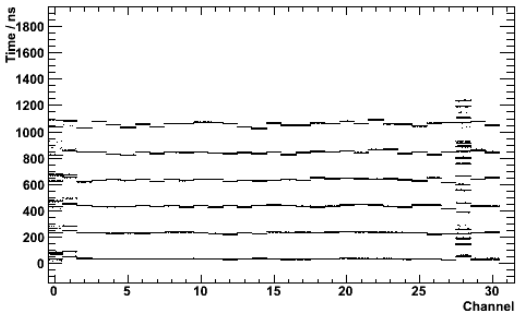

Figure 5.21: Third module: Time peaks distribution for TDC delayed by 200 ns.

Comparing the distributions of first layers the difference between the delays of 160 ns and 200 ns cannot be seen easily, but the straw mask for 160 ns-delay shows more broken straws than the 200 ns, figures 5.28 and 5.29.

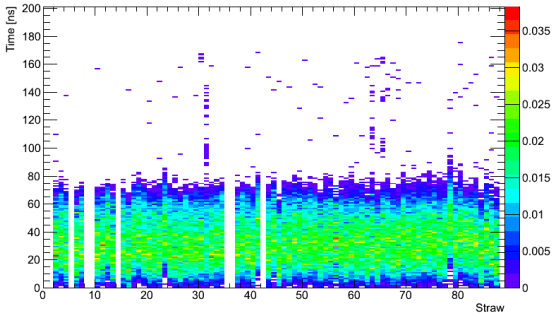

Figure 5.22: Calibration with test pulses for bottom module, first layer for a delayed by 160 ns.

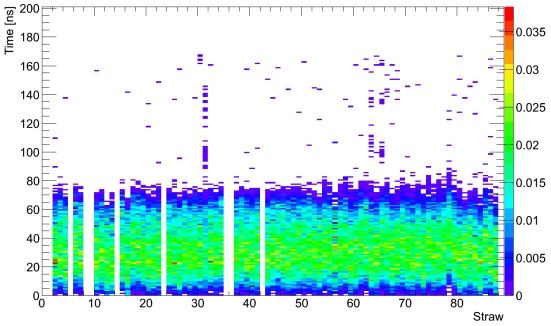

Figure 5.23: Calibration with test pulses for bottom module, first layer for a delayed by 200 ns.

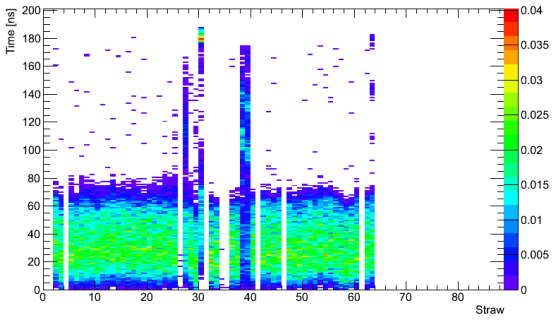

Figure 5.24: Calibration with test pulses for middle module, first layer for a delayed by 160 ns.

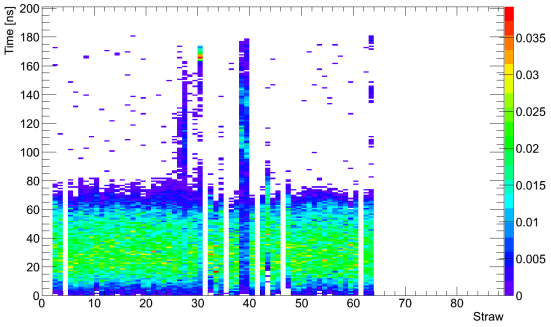

Figure 5.25: Calibration with test pulses for middle module, first layer for a delayed by 200 ns.

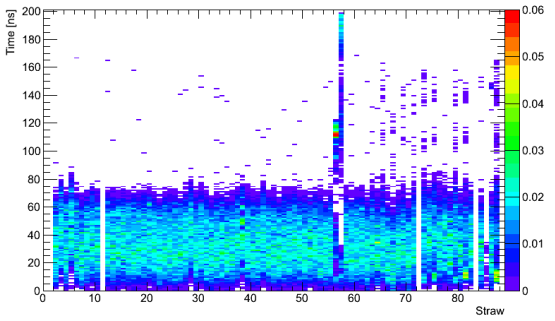

Figure 5.26: Calibration with test pulses for top module, first layer for a delayed by 160 ns.

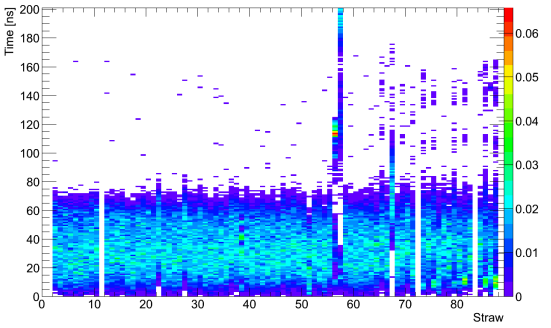

Figure 5.27: Calibration with test pulses for top module, first layer for a delayed by 200 ns.

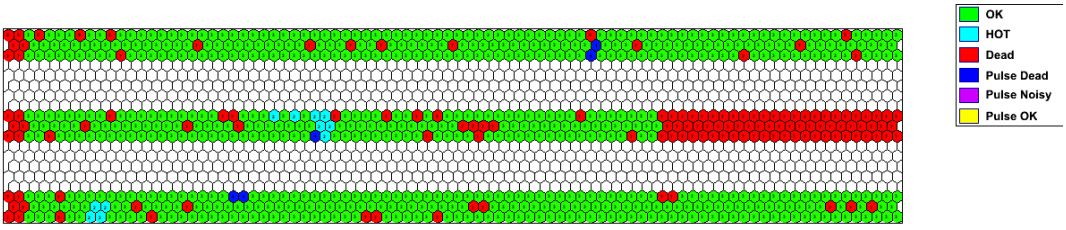

Figure 5.28: Third module: Straw mask for all three modules for test pulses delayed by 160 ns.

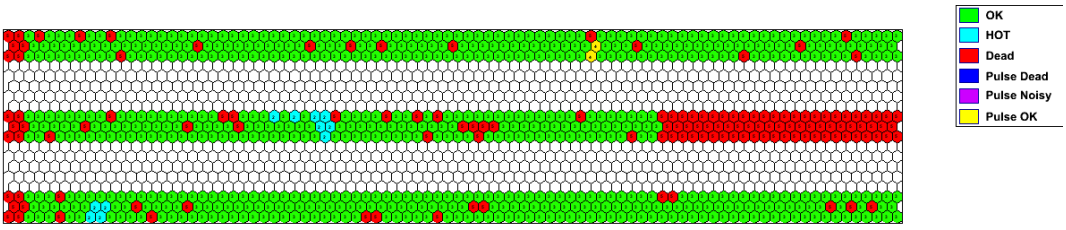

Figure 5.29: Third module: Straw mask for all three modules for test pulses delayed by 200 ns.

5.3.3 First attempt at FE board-by-FE board calibration

Changing the calibration in the way that calibration would be performed FE board-by-FE board and not straw-by-straw anymore turned out to be more difficult, as the calibration software is written for a straw calibration and in a way that it is difficult to rewrite. First, information on the hits from all the straws in one FE board are combined and written back to the straws. That way all the straws contain the same information on drift times and the distribution in all straws in a FE board are the same. The examples before the calibration are presented in figures 5.30 - 5.32 for the first layer of all modules and the remaining distributions can be found in the appendix in figures A.25 - A.30.

Combination of the straws of one FE board was successful. The distribution is strongly pronounced for different FE boards. The red region in the distribution shows the region were the most entries of the single distribution are gathered. This region should have the width of a typical distribution of $\approx 80\,\text{ns}$. The highest value set in the calibration for the distribution is 120 ns. The red region in the middle module is barely in the range, so that not the whole FE board will be marked as hot. The noise in the background is also pronounced more strongly as well. With more events it could mean that the distribution became too broad and the whole FE board would be marked as hot after the calibration is finished. To prevent writing the distribution of the hot or continuous straws to the drift time distribution for all other straws, so that distribution for the FE board gets too broad, the quality of the straws was checked before gathering the distributions. However, it did not help to cut all the extra noise hits.

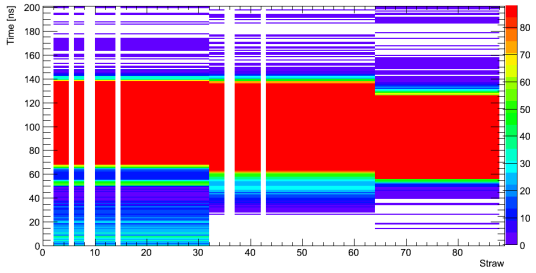

Figure 5.30: Distribution of the drift time for each front-end board using the test-pulse calibration: bottom module, first layer

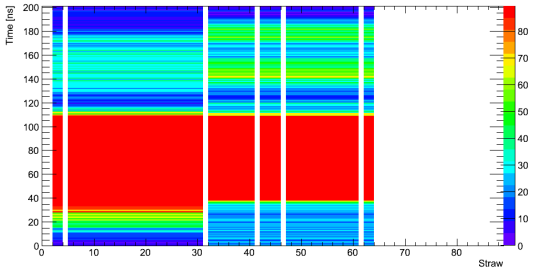

Figure 5.31: Distribution of the drift time for each front-end board using the test-pulse calibration: middle module, first layer

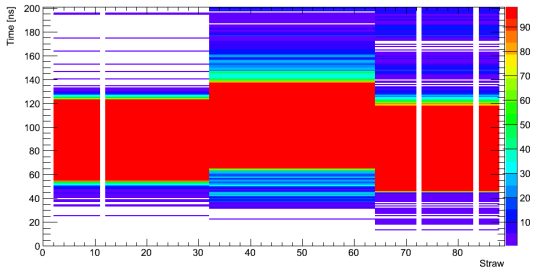

Figure 5.32: Distribution of the drift time for each front-end board using the test-pulse calibration: top module, first layer

Figures 5.33 - 5.35 normalized distribution for the first layers of all modules after the calibration is shown. The calibration is still performed straw-by-straw, so it is using the same distribution for the straws in one FE board, not all the straws are shifted to the same starting point. Changing way of the

calibration did not improved the calibration, even made it worse. However, the distribution of the FE boards shows a clear line, so may be it can be improved further with more studies.

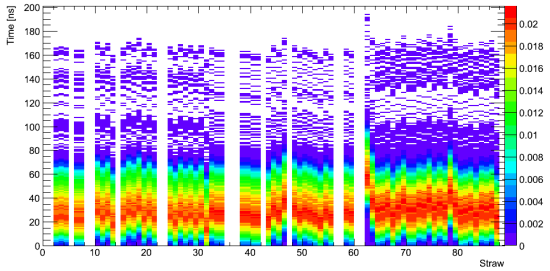

Figure 5.33: Test pulse calibrated data for FE boards in bottom module, first layer

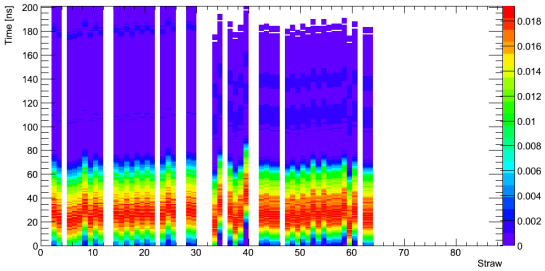

Figure 5.34: Test pulse calibrated data for FE boards in middle module, first layer

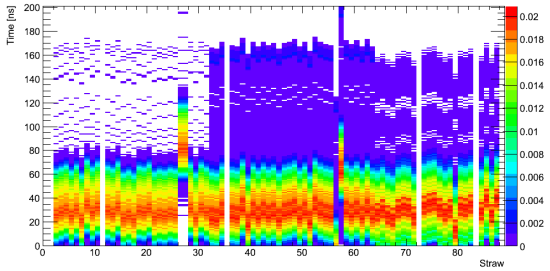

Figure 5.35: Test pulse calibrated data for FE boards in top module, first layer

5.3.4 Studies with the middle module: efficiency and residuals

With the data gathered with the middle module, the studies of how efficient a straw in a module is can be performed. The information about the hits in the events from the top and bottom modules is used to reconstruct the tracks of the particles. Information about the hits are stored for the middle module as well, but are not used for the reconstruction. Comparing the information about the position of the hits in the middle module it can be concluded if the middle module was aligned properly.

The reconstructed track is also crossing the middle module. Hence hits are expected along the track in the middle module as well. To study the efficiency of a straw the different combinations of number of hits are analyzed. Along the track three hits are expected, but other combinations are also possible. The most likely cases, with 1,2, or 3 hits along the track, are presented in table 5.1. "Expected" means number of expected hits along the track and "measured" is number of the hits along the tracks that were reconstructed. In table 5.1 events with 5,6 or 7 hits are added up and represented as the first entry of the table. These cases are much more less likely to happen, because it would mean that the particle entered at very high angle. To cross at least 5 straws the angle should be higher then 50° and the track is difficult to register to due to construction of the detector. However, this number is small enough compared to the other cases and can be neglected in the calculation. In the table 5.1 the distribution of the number does not look too good, because the whole middle module is used for the calculation. Since the short FE board is not connected and hence no information on hits in these straws is stored there are many hits that are expected but not measured. Therefore analysis was repeated with focus only on a smaller part of the modules which contains few broken straws. Straws from 45 to 64 were chosen for this study. To stay in this range the calculation was repeated for tracks with angles smaller then 30°. As the possibility to have more then one track is rather small there were no cuts set on the number of tracks. New, larger data set was recorded and analyzed to for further studies. The results are summarized in table 5.2. As one can see, the numbers of hits for all but three expected hits along the track are negligibly small. Also there are no entries for tracks with more then 4 hits. It verifies the theory that only tracks with angles higher then 30° would cross more then 4 straws.

Expected /Measured	0	1	2	3	4
0	308	–	–	–	–
1	0	7	–	–	–
2	46	121	270	–	–
3	1526	1352	5717	4111	–
4	144	180	346	313	72

Table 5.1: Number of tracks with a given number of expected and measured hits in all the straws of the middle module.

In figures 5.36 and 5.37 for data and Monte Carlo simulations, respectively, the numbers from table 5.1 are presented as a 2D histogram. There are also other possible combinations plotted besides the ones in figure 5.1, but as the numbers are not that high these combinations are neglected.

The efficiency can be calculated using the binomial test of statistical significance of probability theory. The efficiency of a straw can be then can calculated using the probability mass function 5.1:

$$P = \binom{n}{k} \epsilon^k (1-\epsilon)^{n-k} \tag{5.1}$$

with

Expected /Measured	0	1	2	3	4
0	–	–	–	–	–
1	0	1	–	–	–
2	0	35	196	–	–
3	0	582	5734	7020	–
4	0	103	540	765	208

Table 5.2: Number of tracks with a given number of expected and measured hits in the region with mostly good straws of the middle module.

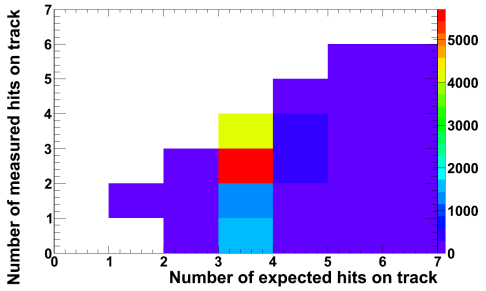

Figure 5.36: Efficiency of reconstructed hits for cosmic data.

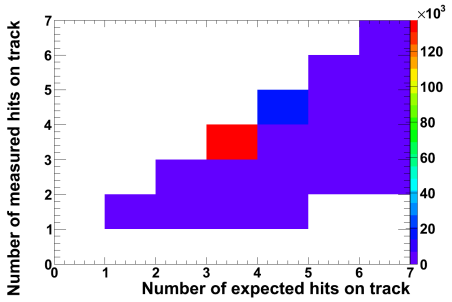

Figure 5.37: Efficiency of reconstructed hits for Monte Carlo simulation before implementation of dead and hot straws.

- n: number of expected hits
- k: number of measured hits
- ϵ: efficiency of a straw

A new sample with more events was used to calculate the efficiency to receive more precise results. The case for 3 expected and 3 measured hits along the track has the most entries, the next most likely case is with 3 expected and 2 measured case. Those two cases are chosen to calculate the efficiency with equation 5.1. First of all:

$$P = \binom{3}{3} \cdot \epsilon^3 = \epsilon^3 = \frac{7020}{N_{\text{track}}}$$

with N_{track} the number of all tracks, and

$$P = \binom{3}{2} \cdot \epsilon^2(1-\epsilon) = 3 \cdot \epsilon^2(1-\epsilon) = \frac{5734}{N_{\text{track}}}$$

As we expect the efficiency to be the same for all the straws, with those two equations we can calculate ϵ:

$$\frac{P_{\binom{3}{2}}}{P_{\binom{3}{3}}} = \frac{5734}{7020} = 0.817 = \frac{3 \cdot \epsilon^2(1-\epsilon)}{\epsilon^3}$$

$$\frac{3 \cdot (1-\epsilon)}{\epsilon} = \frac{5734}{7020}$$

$$\epsilon = \frac{7020}{\frac{5734}{3} + 7020}$$

$$\Rightarrow \epsilon = \frac{3}{3.82} \approx 0.786$$

The efficiency of a straw in a module is around 80%. The error can be calculated as follows:

$$\Delta\epsilon = \sqrt{\frac{\epsilon \cdot (1-\epsilon)}{5734 + 7020}} = 0.005$$

which gives us an efficiency of $\epsilon = 0.785 \pm 0.005$.

The same way the efficiency can be calculated using other combinations of measured to expected hits in the straws, for example comparing the numbers for finding two or only one hit on track.

$$P = \binom{3}{2} \cdot \epsilon^2(1-\epsilon) = 3 \cdot \epsilon^2(1-\epsilon) = \frac{5734}{N_{\text{track}}}$$

and

$$P = \binom{3}{1} \cdot \epsilon(1-\epsilon)^2 = 3 \cdot \epsilon(1-\epsilon)^2 = \frac{582}{N_{\text{track}}}$$

$$\frac{P_{\binom{3}{1}}}{P_{\binom{3}{2}}} = \frac{582}{5734} = 0.101 = \frac{3 \cdot \epsilon \cdot (1-\epsilon)^2}{3 \cdot \epsilon^2 \cdot (1-\epsilon)}$$

$$\frac{(1-\epsilon)}{\epsilon} = \frac{582}{5734}$$

$$\epsilon = \frac{5734}{582 + 5734} \approx 0.908$$

$$\Rightarrow \epsilon \approx 0.908$$

$$\Delta\epsilon = \sqrt{\frac{\epsilon \cdot (1-\epsilon)}{582 + 5734}} = 0.004$$

The efficiency calculated this way is even better then before $\epsilon = 0.908 \pm 0.004$, which means it is around 90%.

The calculated efficiency for both cases are too far apart, the difference is more then 10%. The efficiency is expected to be the same for all straws. Such a big difference occurs due to the dead straws. Though a region with only few problematic straws was chosen, there are still straws that are not used in reconstruction, so that it is more likely to have a track with two reconstructed hits than with three.

The same way the efficiency in Monte Carlo simulation can be studied as well. In figure 5.37 the distributions of the possible combinations of measured to expected hits in the middle modules shown, with expected the number of hits on track expected to be found and measured the number of hits reconstructed along the track. In table 5.3 the numbers for all most likely possible combinations are summarized.

The combinations for 3 hits are chosen, because it is the most likely case in which a segment from the hits can be reconstructed. Also the numbers for 1 or 2 hits are few, but unexpectedly high for 4-to-4 case, as it is difficult for a particle to pass through 4 straws at the same time. After the same calculation as described above for the cosmic data the following results are obtained.

Expected /Measured	0	1	2	3	4
0	–	–	–	–	–
1	0	0	–	–	–
2	0	0	110	–	–
3	0	17	96	10434	–
4	0	1	120	222	3104

Table 5.3: Numbers for calculating the efficiency of a straw in the middle module.

For $P_{\binom{3}{2}}$ to $P_{\binom{3}{3}}$ $\epsilon = 0.997 \pm 0.001$, which means it is around 100% and $P_{\binom{3}{1}}$ to $P_{\binom{3}{2}}$ $\epsilon = 0.849 \pm 0.034$, which means it is around 90%. The efficiency in the simulation is definitely too high compared to data which is another proof of necessary improvements in Monte Carlo simulation. The simulation does not consider the dead straws in the modules or the geometry of the setup. In fact in such a case one would expect a perfect reconstruction of hits, so there should not be any events with one or two out of three reconstructed hits. Though, reconstruction software is not perfect. It is still possible, that the reconstructed track is shifted a little. Then a track would cross a straw with no hit in it.

After implementing information about dead and hot straws the following numbers were received:

Expected /Measured	0	1	2	3	4
1	0	0	–	–	–
2	0	15	69	–	–
3	70	257	752	1959	–
4	4	42	85	167	480

Table 5.4: Numbers for calculating the efficiency of a straw in the middle module.

The efficiencies are now $\epsilon = 0.872 \pm 0.006$ and $\epsilon = 0.745 \pm 0.014$ for the same measured-expected combinations. The same big difference for efficiency calculated for $P_{\binom{3}{2}}$ to $P_{\binom{3}{3}}$ and $P_{\binom{3}{1}}$ to $P_{\binom{3}{2}}$ is observed. This behavior should be studied more closely in the future studies.

The results are demonstrated in the table 5.5.

		ϵ for $\binom{3}{3}$ to $\binom{3}{2}$	ϵ for $\binom{3}{2}$ to $\binom{3}{1}$
Data		0.785 ± 0.005	0.908 ± 0.004
MC	old	0.997 ± 0.001	0.849 ± 0.034
MC	new	0.872 ± 0.006	0.745 ± 0.014

Table 5.5: Numbers for calculating the efficiency of a straw in the middle module.

The residual for the MC simulation was also studied. Before implementation of information on dead and hot straws residual looked like in figure 5.39, a peak around 0, which means that there was almost no difference between the simulated and reconstructed track. After setting the smear value to 1.65 mm and implementation of dead and hot straws into Monte Carlo simulation improved residual is now looking as shown in figure 5.40. There distribution is broader, but there is still a huge difference to data.

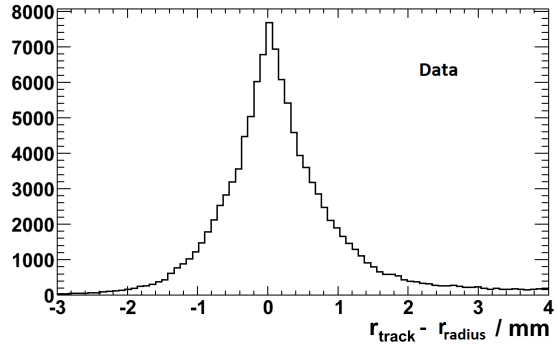

Figure 5.38: Third module: the difference between the track distance to the wire and the reconstructed drift radius.

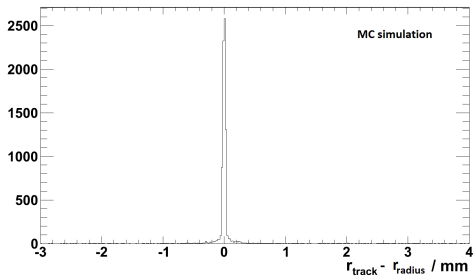

Figure 5.39: Third module: the difference between the track distance to the wire and the reconstructed drift radius for Monte Carlo simulation before improvements.

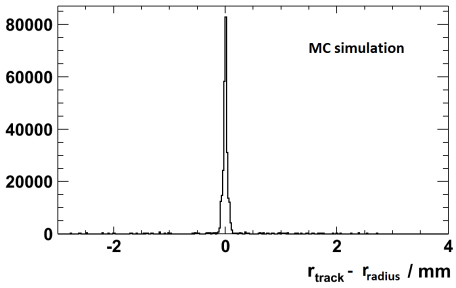

Figure 5.40: Third module: the difference between the track distance to the wire and the reconstructed drift radius for Monte Carlo simulation after improvements.

CHAPTER 6

Software developments

The software used to work with the data received from the experiment was already described shortly in the chapter 3. In this chapter the software and performed changes will be described in more detail. The biggest changes were made in the reconstruction part of the software. But the general refactoring was applied to all parts of the software. A major refactoring was needed to allow the usage of the third module since the software was written for only using two modules. The second step was to improve the angular distribution for the tracks. First, the study of the unfavorable angles was performed to determine for which angles it is more likely that the hits cannot be reconstructed, or the segments are reconstructed wrongly. Then the different ways of improving of the reconstruction can be tested. For this purpose, the idea of creating more then one segment for the same hits in one event was developed. The next step was to improve the reconstruction of the hits with the more precise way of reconstructing of the drift radius from the drift time.

After the studies performed with the middle module, the Monte Carlo simulation can be adjusted to describe the data more closely then it did before. The reconstruction and analysis software work the same way for Monte Carlo simulation as for the cosmic data. The only differences are in the way the data files are created and processed. That is why, Monte Carlo simulation gets treated similar to data but still separated.

6.1 Code refactoring

Refactoring means changing the code so it gets faster and more efficient, but also easier to read or change and adjust for the possible changes in the future. The code is divided in six main parts. Each part has its own task to fullfill. There is one part that is responsible for simulation; the other is responsible for the geometry of the detector, then one for analysis and reconstruction and creating the histograms, as well as one the reconstruction of the hits, segments and tracks, the software to decipher the raw data and converting it to the file which stores the information about the event and the calibration software. Each part consist of many different files, which has to be handled carefully since all the parts of the code share the variables. One of the purposes of refactoring is to avoid such variables, so the parts of the software can be changed more easily.

6.1.1 Third module implementation

The refactoring started with rewriting of the class that describes the setup and its geometry. The information about the distance between the modules, the number of straws, straw radius, number of front-end boards and others is stored there. The geometry class is a part of the software which stores the information on the geometry of the experiment. When an event occurs it is stored temporarily in the memory with geometry information from this class about position of the reconstructed hit, segment or track. This geometry class was first a namespace and had the two modules hard coded. It means everywhere, where the information about where the hit occurred where called, it was done by calling the top or bottom module. With the assembling of the middle module the problem was that there were no information about the middle module, its position or to which FE board or TRB it is connected, so no information from the middle module could have be received since for the software it did not existed at all. The namespace was changed to a class, which received an object for the last and first module. The top module is then set equal to the number of modules. For example, after installation of the middle module, the number of the top module is set to 3, because the counting starts with the bottom module. Now, the modules can be called as first or last, or for the modules in the middle as combinations from those objects (for example "last module - 1"). Also, with the middle module the distance between the modules has changed. It is also considered while refactoring and a line with the information on the distance between three as well as one for two modules was added. With these changes the number of the modules can be changed as many times as necessary. If it is needed to go back to using only two modules, the number of the top module should be set to 2 and the line with information about the distance between two modules should be used instead of the one for three modules. Two more classes were added to the geometry class to simplify the access to straws with hits.

6.1.2 Segment candidates

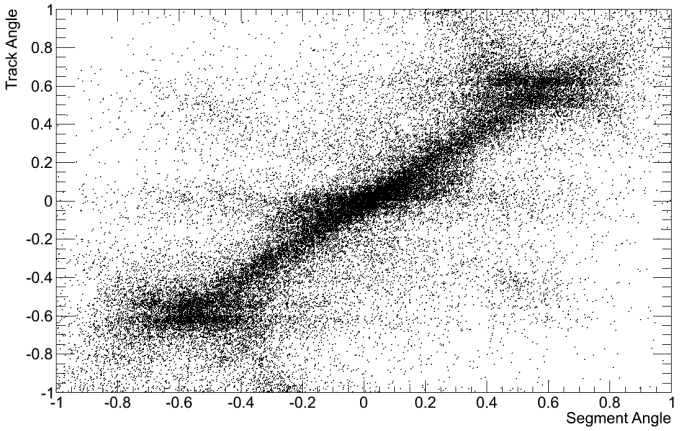

Figure 6.1: A 2D histogram of segment slope vs track slope.

To improve the angular distribution further studies of the angles of the reconstructed segments and tracks are needed. In figure 6.1 the angles of the reconstructed segments versus the angles of the tracks reconstructed from those segments are plotted. Expected is a distribution along the diagonal, if the segments reconstructed for all the angles equally. But there are more entries around 0 and 0.6. The particle passed the detector and the hits were reconstructed, but by the reconstruction of the segment a

segment with wrong angle was reconstructed.The same problem can be seen in figure 4.11. There are peaks strongly pronounced for a specific angle. To understand this problem the following figure 6.2 was created and studied closely.

There is a distance between the straws, though it is kept minimized. If the charged particle crosses the module in a way that it passes these distances it is likely that the track would not be reconstructed. To reconstruct a track at least 3 hits together are needed and if one or two are lost due to the missing ionization in a straw the track cannot be reconstructed. On the other hand, it is possible that the particle had crossed the straw but too close to the tube. The path of the track is too short and gas cannot be ionized. Information from this straw is also lost and no segment can be created. In figure 6.2 red lines represented possible segments for unfavorable incident angles. After a few test and further analysis the most unfavorable angle was determine to be 17°. That explains the dips in figure 4.11.

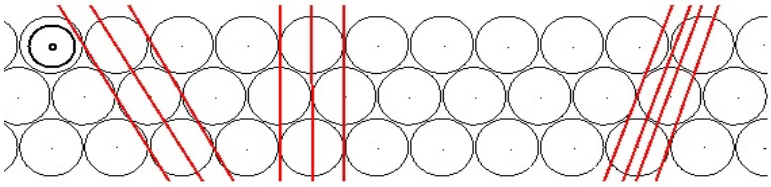

Figure 6.2: Studies of the unfavorable angles of the tracks. A schematic representation of possible segments (red lines) in a module. Segments which cross the module between the straws or straws too close to the tube cannot be reconstructed.

From figure 6.1 can be concluded that there are many segments which have wrong angle. The software for display of the events mentioned before in chapter 3, SED, offers a good possibility to study this problem. Many events can be simulated and studied easily and, if needed, reloaded again or a new set simulated. After simulating and creating many different sets of the events a similarity was detected presented in figure 6.3. In this example for the particle passing on the left side the hits were reconstructed correctly and there are also segments created using those hits, but the track could not be reconstructed, because the segments were reconstructed with a wrong angle. It seems that there is angle which is preferred while reconstructing a segment.

As mentioned before there are two segment creating algorithms, the first one uses three hits one in the middle layer and two from the neighbor straws from top and bottom layers, and the second one is also using at least three hits, but checks four nearest straws in top and bottom layer and two straws next to the straw with the hit. The segments are reconstructed by fitting a tangent to the hits. First, the hit in the middle layer of the module is found. From this hit the neighbor straws in the top and bottom layers are checked if there is a hit. If hits in at least two neighbor straws are found, the segment can be created. The fit starts with a line at one side of hits. In small steps a line is refitted to the hits until the software finds one line with the smallest χ^2 of the slope. The next line would have a higher χ^2 which indicates that the best segment was found and this line stored as the segment. As the software stores the first best segment and breaks off the scan, the possible segment on the other side of hits would not be found, like this is the case in figure 6.3. The stored segment is a tangent to all three hits, but there is a possible segment, which was not reconstructed, in the direction of the represented track.

Though for MC simulation there is no problem with the distances between the straws, as simulation does not consider that in the real detector there are distances between the straws. In figure 4.11 the distribution for simulation is shown in red. The dips are less pronounced, but there are still peaks around 0 and 0.6. Since the reconstruction of the segments is performed by the same code, wrong

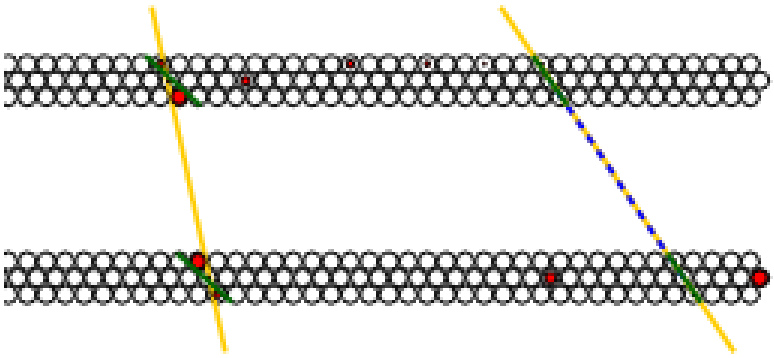

Figure 6.3: Simulation example of wrong reconstructed segments. The green lines are segments, the blue dashed line is reconstructed track. Red circles are the drift circles.

reconstructed segments occur in MC simulation as well.

The first approach was to test for the first algorithm if the tangent with the smallest χ^2 is not the right segment, then may be the second best χ^2 would solve the problem. For this purpose segment candidates were created. The search for the hits starts again in the middle layer and then checking the top and bottom layer for the neighboring hits. If there are more then three found, the tangent is fitted to the hits, but this time the tangent with smallest and second to the smallest χ^2 are stored as segment candidates. In the same way the hits in the other module are tested and the segment candidates are created. In order for the segments not to be used twice, the segments were grouped together and if one of the segment was used to created a track the other segment from the same group was discarded. An example of such segment candidates is shown in the figure 6.4.

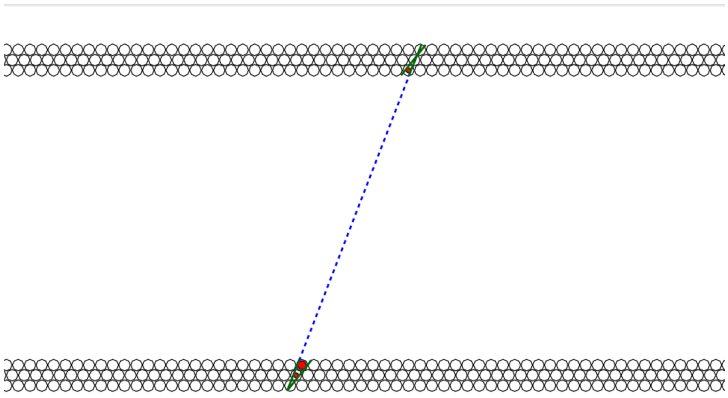

Figure 6.4: Simulation example of reconstructed segment candidates. The green lines are segments candidates, the blue dashed line is reconstructed track. Red circles are the drift circles.

6.1.3 Improving of the segment candidates

The segment candidates helped to improve the distribution a little. But there are still cases where the best slope and the second best slope are only slightly different. In that case the difference of the slopes is so small that cannot be separated in SED. The position of the segment respectively to the hits does not change as well. The segment candidate is on the same side of the hits and still has the wrong angle. That why, it was decided to improve the segment candidates method further. As the two segments are constructed for the same group of the hits, but have to be placed on different sides of the hits, the next step is to store one segment with the smallest slope and information about its position around the hits. To achieve that further refactoring was performed.

The segment candidates method is first changed so the segments are created on both sides of the hits. It is done the same way like before, but now the software checks if the segments are sharing any hits and if yes it constructs the possible segment on the other side of the hits. By doing that the problem with two inseparable segments is solved. It is also possible to create as many segment candidates as wished by just changing one number in the code.

Now the candidates share the same hits but not sorted into groups. It means all the segments are used to create a track. That leads to the next problem displayed in figure 6.5. Each the segments from bottom module is connected to all the straws in the top module and vice versa. In the event shown in figure 6.5 only two tracks were simulated but at least 5 reconstructed. A method to separate the segments and the tracks is needed, so that no unnecessary tracks will be reconstructed or spare tracks can be recognized and deleted. However, this required further refactoring of the code. The only difference between the tracks were the segments and the segments were reconstructed using hits, but no information about the hits was stored. The same applies to the tracks, no information on segments or hits were stored or even the χ^2 of the track. It made it difficult to chose between the tracks. During the refactoring a class SFittedLine was added, which, as the name says, is responsible for fitting the lines, tracks or segments, and storing the information on χ^2, slope, number of hits, position etc. With this information there are more possibilities to set a few criteria, which can be used to distinguish between the tracks. There are 6 different criteria to chose from, three for hits and three connected to χ^2. The hit criteria is checking if the tracks sharing the same hits and how many. If all the hits are the same, one of the tracks can be deleted. The next criteria which compares χ^2 then decides which of the tracks is kept and which deleted. There were following criteria created: shared or unique hits and hit topology. Shared hits checks if the hits are the same hits in the same module and for the same group of hits in event, which would mean that both segment candidates are used to reconstructed a track. Then one of the tracks can be deleted. Unique hits criteria checks if the segments are coming from the same group of hits, and if not, the segments are not the segment candidates, but actual segments, using the hits caused by two different particles. Hit topology criteria compares if the segments used for tracks are coming from the same side of the hits, again to decide if actual segments or segment candidates from the same group of hits are used. One of the χ^2 criteria is then used to decide, which of the tracks is stored. There are also three possibilities to use. First, simple compares the χ^2 of the tracks and the one with the smaller χ^2 is kept. The second criteria checks the χ^2 and calculates the number of hits used to reconstruct the track, then decides based on better χ^2. The last one works the same way as the second criteria, but for the decision is more important, how many hits are used. For the higher number of used hits it is more likely to reconstruct the segment, and then the track correctly.

In figures 6.6 - 6.7 the angular distribution of the track slope for data on the left and for simulation on the right are presented, after implementing the improved segment candidate method. The distribution is smother, the peaks are almost vanished for data and completely gone for simulation. In data there are still more events around 0. This cannot be changed by software. At -0.6 the distribution rises and at 0.6

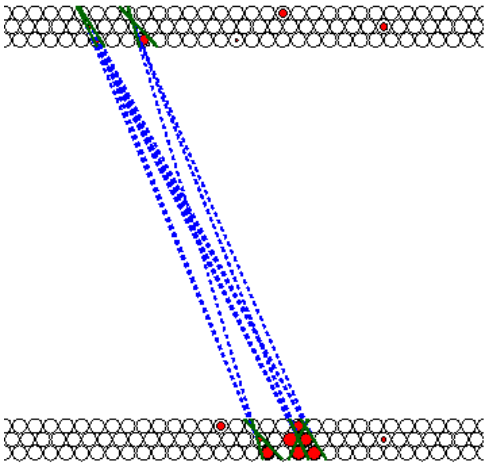

Figure 6.5: An example of an event with too many tracks reconstructed.

falls abruptly. This region is covered by scintillators, so that it is more likely to register an event in this region.

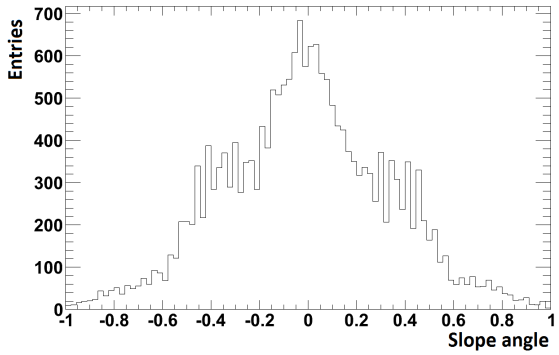

Figure 6.6: The slope distribution of the reconstructed tracks for cosmic data.

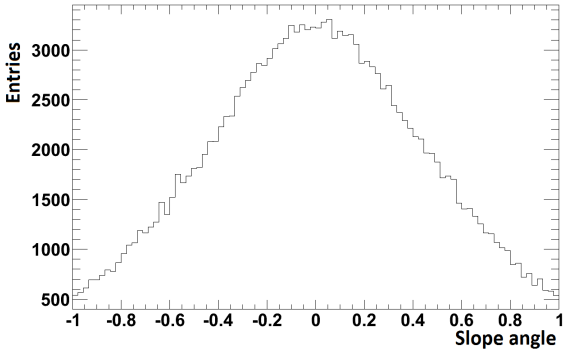

Figure 6.7: The slope distribution of the reconstructed tracks for Monte Carlo simulation.

6.1.4 Monte Carlo simulation improvements

Improving of the MC simulation was done in many steps. Besides the already mentioned in section 5.3.4 presented changes implemented in the simulation itself, which are the number of dead and hot straws in the simulation and adjusting of the smear value of the drift radius, there are also other modifications of the code that were performed. Additionally there is, of course, the improved segment candidates method presented earlier in this chapter which influences simulation as well. Another step was to change from the linear drift time - drift radius dependence to the one used in ZEUS STT. The shape is more S-like shape than a linear function. The drift time depends on the gas mixture used in the detector. From ZEUS experiment a documentation on the measurements of the drift times for different gas mixtures were obtained (see appendix A.5). In STYX a mixture of 80:20 for Ar:CO_2 is used. The documentation from ZEUS contains the measured points for different threshold voltages. After discussions with the supervisors the dataset for a threshold voltage of 185 eV was chosen. The parameters in ZEUS docu-

mentation were saved as data points, not the actual times and had to be recalculated. To recalculate the drift times and the measured radii given in the document a polynomial of 3rd degree was fitted. The polynomial for data is shown in equation 6.1 and for simulation in equation 6.2.

$$r_{drift} = a \cdot t_{drift}^3 + b \cdot t_{drift}^2 + c \cdot t_{drift} + d \tag{6.1}$$

$$t_{drift} = a \cdot r_{drift}^3 + b \cdot r_{drift}^2 + c \cdot r_{drift} + d \tag{6.2}$$

with:

- t_{drift}: calculated drift time
- r_{drift}: calculated drift radius

The parameters for the data are a = -0.012 ± 0.0002, b = 0.013 ± 0.001, c = 0.023 ± 0.002, d = 0.001 and for simulation a = 139.267 ± 0.0001, b = -73.598 ± 0.001, c = 27.605 ± 0.002, d = -0.281. For data and simulation different equations are used, because in simulation simulated radii are stored and not the drift times. That is why, to calculated the fit parameters for MC simulation the drift time is plotted to the drift radius and for data the other way around. There is no error for the last parameters for both, data and simulation, because it was fixed to perform the fitting.

In figures 6.8 and 6.9 the new drift time-drift radius dependence for the data and simulation are presented. With data and Monte Carlo simulation having the same dependence adopted from the measurements from the earlier experiments is expected to improve the data and MC simulation agreement.

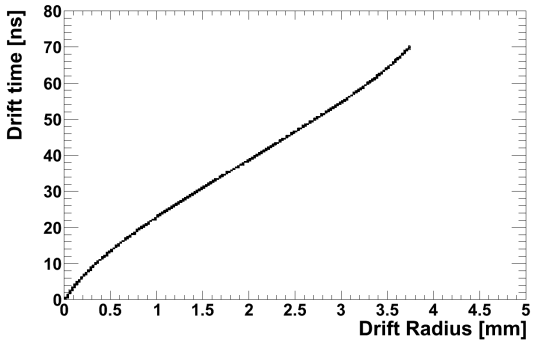

Figure 6.8: Space-drift time resolution for cosmic data after improving.

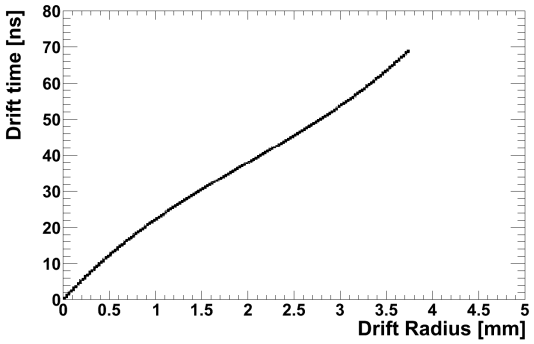

Figure 6.9: Space-drift time resolution for the simulation after improving.

CHAPTER 7

Conclusions and outlook

This study showed the first steps in achieving the desirable improvements of STYX. Throughout the study both software and hardware of the experiment were explored closely. In the fist step, the ideas for the possible developments were gathered. The main studying point was set at the software, reconstruction in the beginning, then studies of calibration were added. Only after performing hardware tests it was decided to modify the hardware.

The most important part of the software is the reconstruction of the tracks, therefore most developments were concentrated on this part of the code. Since angular distribution did not correspond to the expected form, the segment candidate method was developed and implemented. While implementing the new method, a major refactoring of the code was performed. Refactoring of the reconstruction improved the angular distribution for the segments and made the reconstruction of the tracks more precise, but it is also made the code more flexible. The software can be adjusted more easily for possible changes: adding more modules; changing the number of the segment candidates; studying the tracks of the particles etc. It also allows further changes of the software, if needed, or the returning to the old version as well as opens new possibilities for further studies.

Another advantage of refactoring is an improved agreement between data and Monte Carlo simulation. Simulation software became readable and flexible. It allowed to implement important changes to the simulation software and the differences between the actual data and simulation were reduced. Implementing the flaws of the real detector and treating the simulation the same way as data during analysis of the events improved the agreement.

Improving the calibration was a part of the bachelor thesis [19], which concentrated on calibration of the hardware. The results were adopted in this thesis and extended so that the calibration was now performed on two levels. On the first level the hardware calibrated, then the information from the first calibration were implemented and applied to cosmic data. Performing the calibration in two steps disentangles the electronics problems from straws problems and allows to draw a conclusion about the state of the electronics. Also a new kind of calibration (front-end board-by-front-end board) was tested. This calibration still shows a few flaws that can be fixed with further studies. The calibration code was not refactored yet which may help to improve front-end board-by-front-end board calibration.

Calibration and analysis of the additional module was only possible after performing the refactoring. The middle module allows new studies, which can be added to the laboratory course. It is giving an opportunity to gather more information on detector performance, which would be another interesting task for the students. If the middle module is added to the reconstruction of the tracks, it would al-

low implementation of new reconstruction algorithm for the tracks, which could improve the angular distribution further.

STYX still gives many opportunities for further developments, but also stays an important part of teaching at the university. The laboratory course can be extended with new tasks, studies with the middle module or using the test pulses to study the electronics of the experiment.

Appendix

APPENDIX A

Useful information

A.1 First studies of the experiment

A.1.1 Introduction to the experiment

U in V	N_1	N_2	N_3	Average
1700±0.2	238±15	216±15	202±14	219±18
1750±0.2	493±22	495±22	506±22	498±7
1800±0.2	958±31	955±31	1029±31	981±42
1850±0.2	1747±42	1804±42	1738±42	1763±36
1900±0.2	2837±53	2856±53	2857±53	2850±11
1950±0.2	4648±68	4692±68	4634±68	4658±30
2000±0.2	7435±86	7453±86	7436±86	7441±10
2050±0.2	16820±130	16353±128	16847±130	16673±278
2075±0.2	20472±143	20408±143	20531±143	20470±62
2100±0.2	25330±159	25098±158	25110±158	25179±131
2125±0.2	27018±164	26870±164	27094±165	26994±114
2150±0.2	28945±170	29153±171	29197±171	29098±135
2200±0.2	31735±178	31943±179	31370±177	31682±290
2250±0.2	34453±186	34433±186	34393±185	34426±31
2300±0.2	37354±193	37615±194	37239±193	37402±193

Table A.1: Measurement of threshold voltage for top PMT

U in V	N_1	N_2	N_3	Average
1700±0.2	234±15	255±16	266±16	252±16
1750±0.2	355±19	326±18	353±19	345±16
1800±0.2	404±20	413±20	424±21	414±10
1850±0.2	481±22	471±22	411±20	454±38
1900±0.2	512±23	534±23	518±23	521±11
1950±0.2	594±24	526±23	618±25	579±48
2000±0.2	690±26	631±25	636±25	652±33
2050±0.2	724±27	731±27	701±26	719±16
2100±0.2	730±27	708±27	734±27	724±14
2150±0.2	730±27	723±27	699±26	717±16
2200±0.2	704±27	641±25	746±27	697±53
2250±0.2	727±27	676±26	738±27	713±33
2300±0.2	708±27	753±27	725±27	729±23

Table A.2: Measurement of threshold voltage for coincidence

A.2 Hardware developments

A.2.1 Test pulses

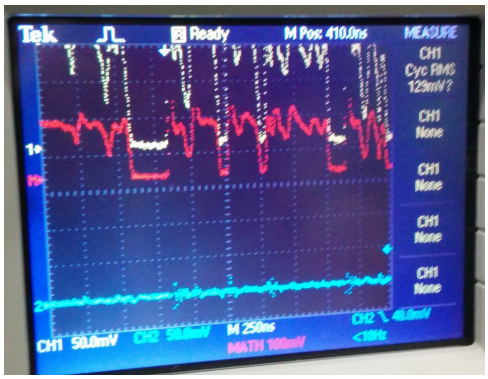

Figure A.1: Test pulses problematic channels for setup at CERN.

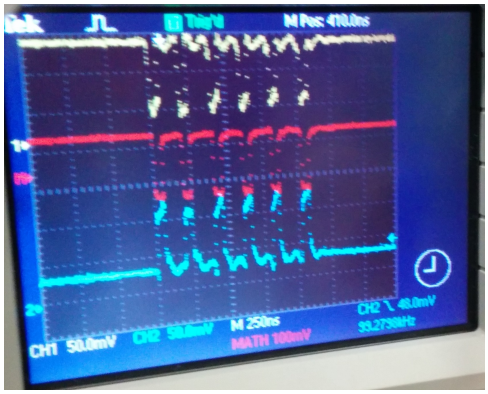

Figure A.2: Test pulses working channels for setup at CERN.

A.3 Calibration

Calibration with test pulses, performed only for two modules:

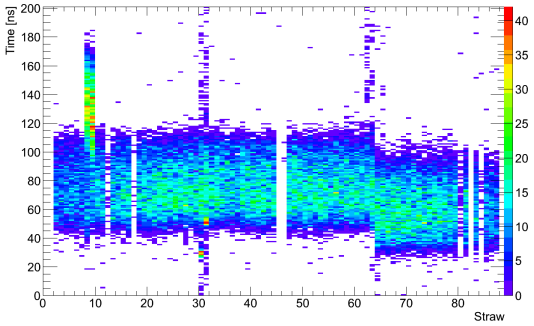

Figure A.3: Test pulse calibration for the bottom module, second layer

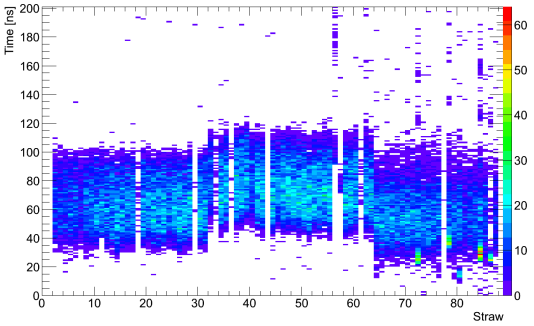

Figure A.4: Test pulse calibration for the middle module, second layer

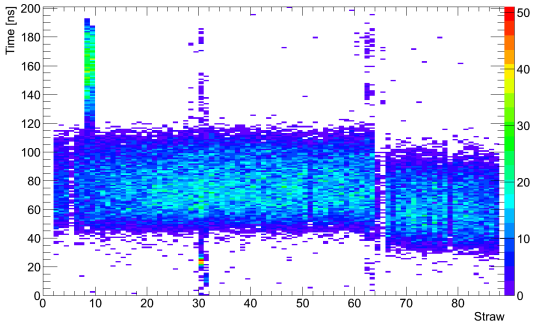

Figure A.5: Test pulse calibration for the bottom module, third layer

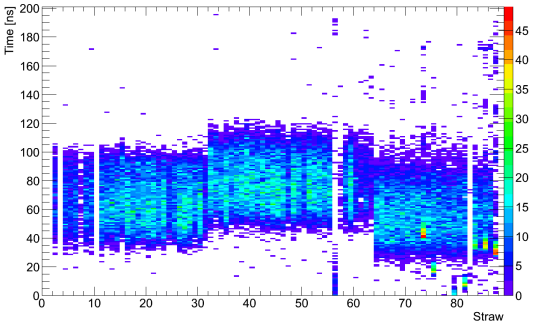

Figure A.6: Test pulse calibration for the middle module, third layer

A.4 Calibration with and without test pulses

Plots for test pulse calibrated data with delay of 60ns:

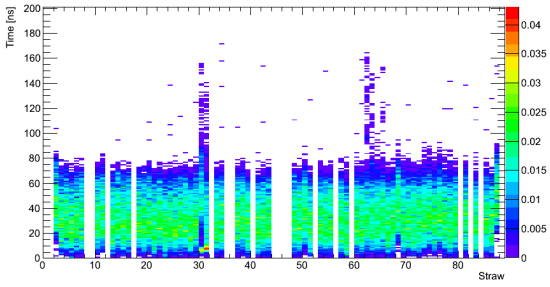

Figure A.7: Test pulse calibration for the bottom module, second layer

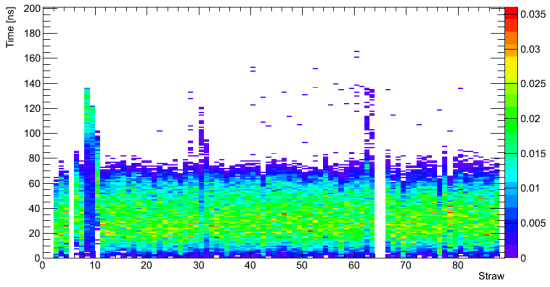

Figure A.8: Test pulse calibration for the bottom module, third layer

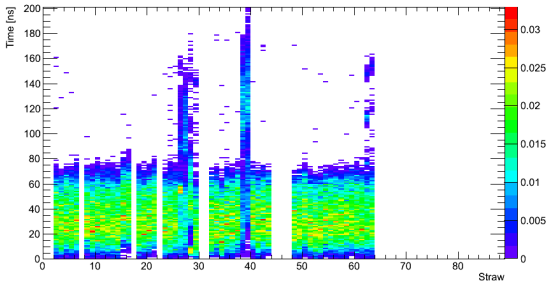

Figure A.9: Test pulse calibration for the middle module, second layer

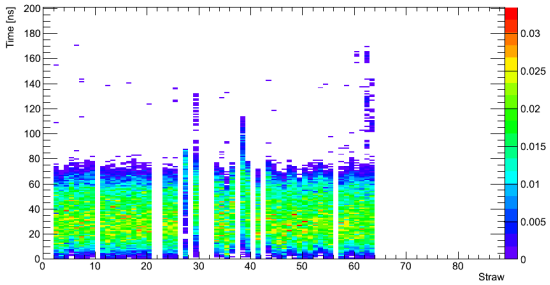

Figure A.10: Test pulse calibration for the middle module, third layer

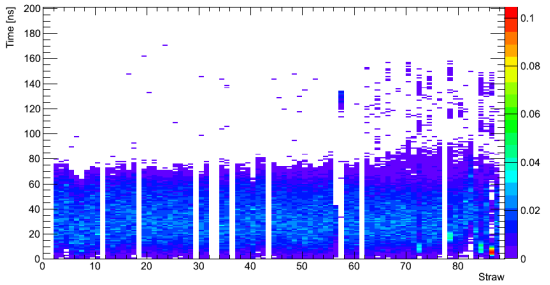

Figure A.11: Test pulse calibration for the top module, second layer

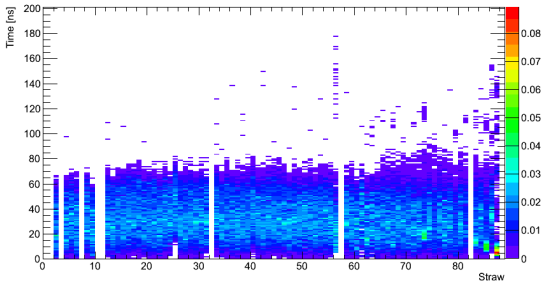

Figure A.12: Test pulse calibration for the top module, third layer

Plots for test pulse calibrated data with delay of 160ns:

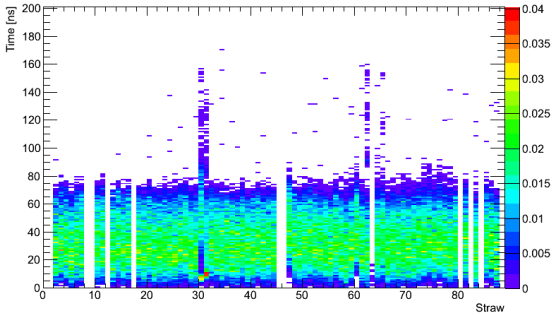

Figure A.13: Test pulse calibration for the bottom module, second layer

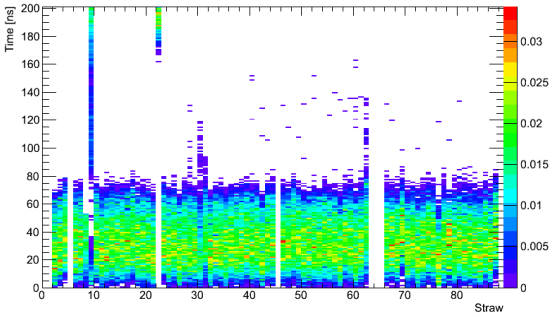

Figure A.14: Test pulse calibration for the bottom module, third layer

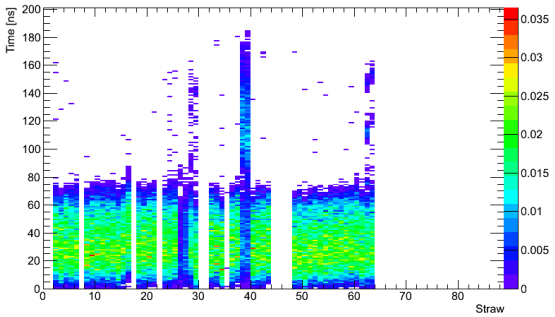

Figure A.15: Test pulse calibration for the middle module, second layer

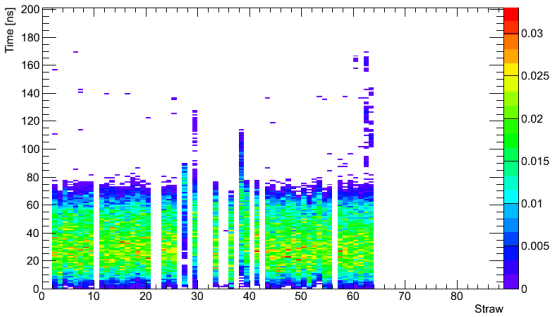

Figure A.16: Test pulse calibration for the middle module, third layer

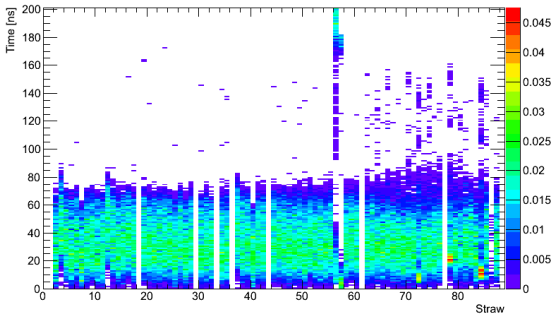

Figure A.17: Test pulse calibration for the top module, second layer

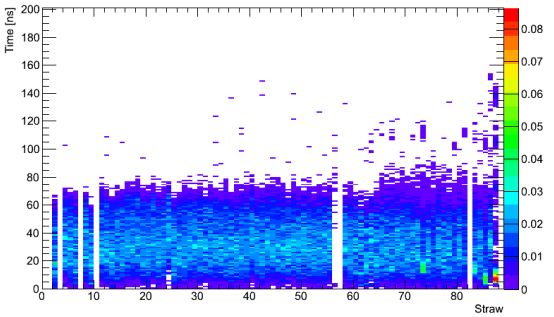

Figure A.18: Test pulse calibration for the top module, third layer

Plots for test pulse calibrated data with delay of 200ns:

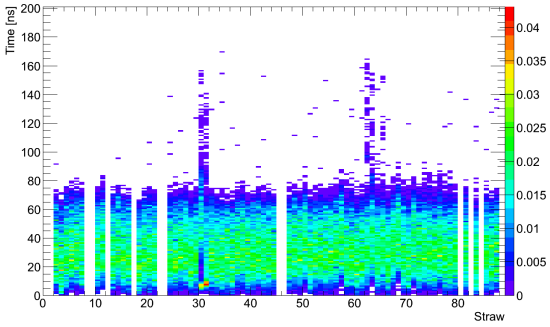

Figure A.19: Test pulse calibration for the bottom module, second layer

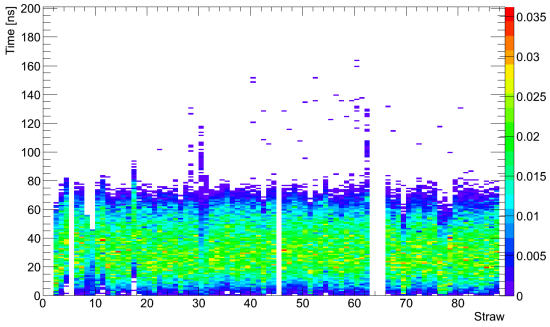

Figure A.20: Test pulse calibration for the bottom module, third layer

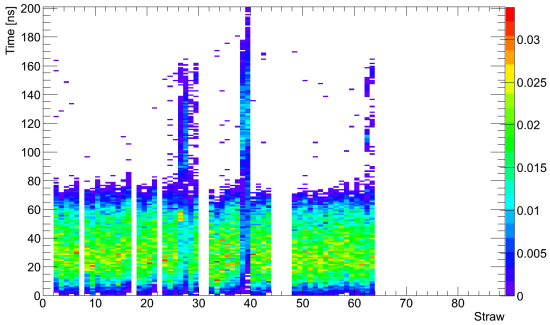

Figure A.21: Test pulse calibration for the middle module, second layer

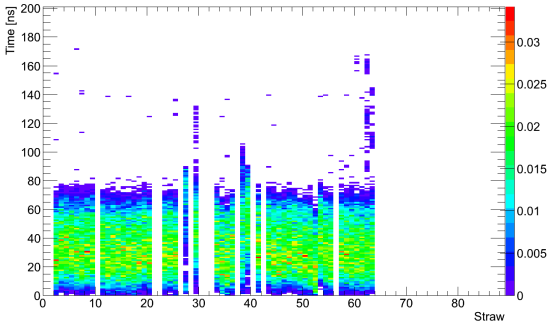

Figure A.22: Test pulse calibration for the middle module, third layer

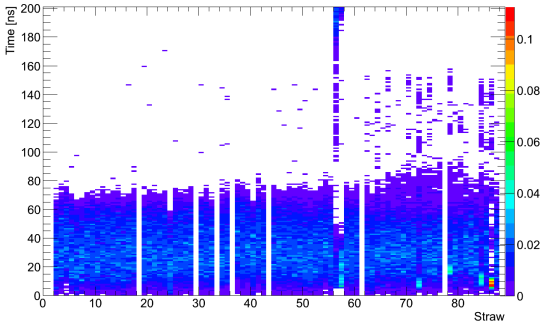

Figure A.23: Test pulse calibration for the top module, second layer

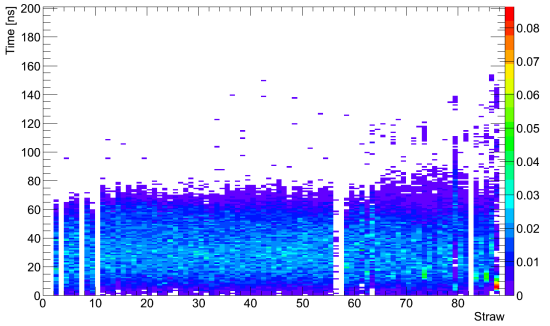

Figure A.24: Test pulse calibration for the top module, third layer

Plots for test pulse uncalibrated data for FE boards:

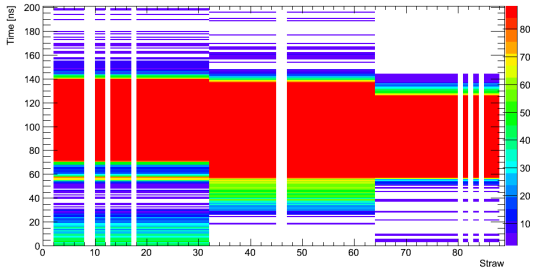

Figure A.25: Test pulse uncalibrated data for FE boards in bottom module, second layer

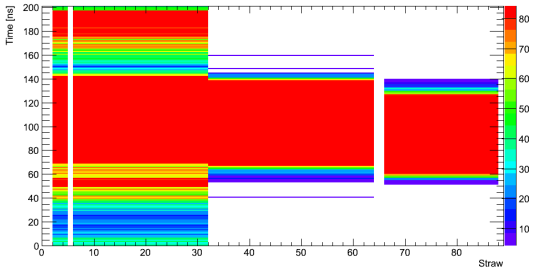

Figure A.26: Test pulse uncalibrated data for FE boards in bottom module, third layer

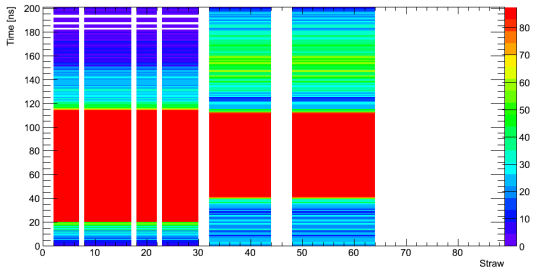

Figure A.27: Test pulse uncalibrated data for FE boards in middle module, second layer

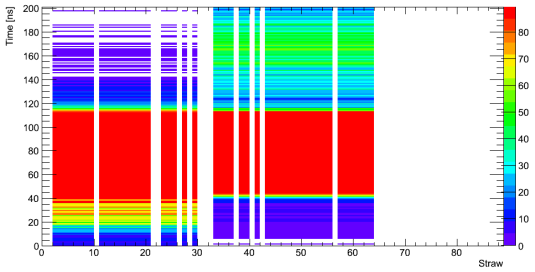

Figure A.28: Test pulse uncalibrated data for FE boards in middle module, third layer

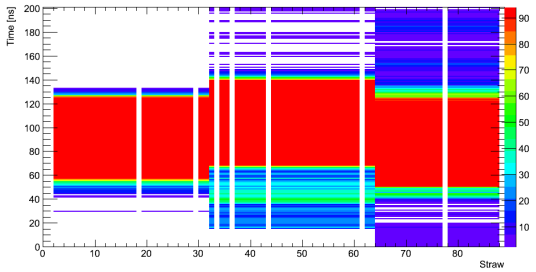

Figure A.29: Test pulse uncalibrated data for FE boards in top module, second layer

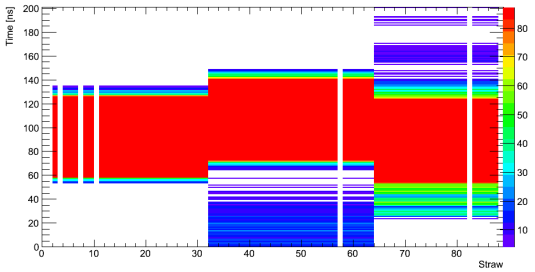

Figure A.30: Test pulse uncalibrated data for FE boards in top module, third layer

Plots for test pulse calibrated data for FE boards:

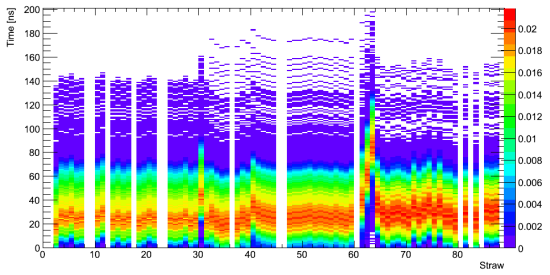

Figure A.31: Test pulse calibrated data for FE boards in bottom module, second layer

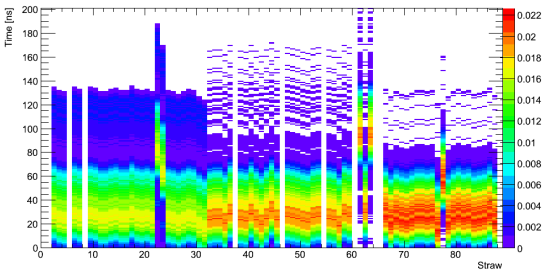

Figure A.32: Test pulse calibrated data for FE boards in bottom module, third layer

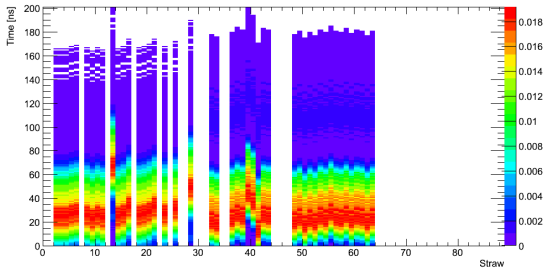

Figure A.33: Test pulse calibrated data for FE boards in middle module, second layer

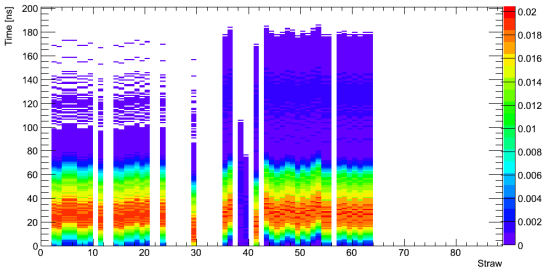

Figure A.34: Test pulse calibrated data for FE boards in middle module, third layer

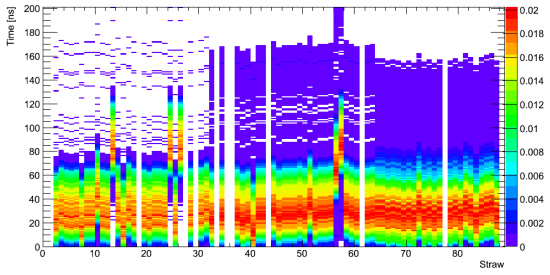

Figure A.35: Test pulse calibrated data for FE boards in top module, second layer

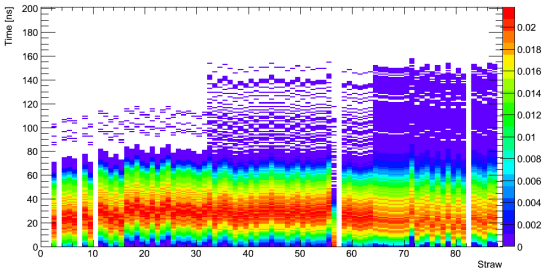

Figure A.36: Test pulse calibrated data for FE boards in top module, third layer

A.5 Drift time calculation informations

```
* strtdep.inc contains a tables of r-t dependence
* for FADC read-out.
c
c R-T dependences after discriminator and FADC
c MEAN values in a slices were used, Threshold = 200 eV
c XENON
Integer NP_Xenon
Parameter (NP_XENON = 11)
Real Time_Xe(Np_XENON),Rad_Xe(NP_XENON)
Data Time_Xe /0., 1., 2., 3., 4., 5., 6., 7., 8., 9., 10./
Data Rad_Xe / 0.0126, 0.0317, 0.0679, 0.1064, 0.1495, 0.197 , 0.2424, 0.2835, 0.3189, 0.3502, 0.3674/

   c.TEST ———————————————————————

   c From DATA
Integer NP_ARGON
Parameter (NP_ARGON = 14)
Real Time_Ar(NP_ARGON),Rad_Ar(NP_ARGON)
Data Time_Ar /0., 0.75, 1., 1.5, 2.0, 2.5, 3.5, 4.0, 4.5, 5.0, 5.5, 6.0, 6.5, 7.0/
* c.1 This set of parameterrs obtained for a threshold = 185 ev
c for hist 507 - after FADC simulation.
c MEAN values in a slices were used
Data Rad_Ar / 0.001, 0.01, 0.03, 0.05, 0.10, 0.13, 0.18, 0.21, 0.25, 0.27, 0.29, 0.33, 0.34, 0.35/

   c.TEST ———————————————————————
C. MC ARGON
Integer NP_ARGON_mc
Parameter (NP_ARGON_mc = 8)
Real Time_Ar_mc(NP_ARGON_mc),Rad_Ar_mc(NP_ARGON_mc)
Data Time_Ar_mc /0., 1., 2., 3., 4., 5., 6., 7. / * c.1 This set of parameterrs obtained for a threshold =
185 ev
c for hist 507 - after FADC simulation.
c MEAN values in a slices were used
Data Rad_Ar_mc / 0.01, 0.05, 0.112, 0.173, 0.234, 0.292, 0.343, 0.37/
   c.2 This set of parameterrs obtained for a threshold = 120 ev
c for hist 507 - after FADC simulation.
c MEAN values in a slices were used
c Data Rad_Ar / 0.0171, 0.047, 0.1051, 0.167, 0.2296, 0.2903, 0.3419, 0.3652/
c.....
```

Bibliography

[1] C. Gruppen, *Astroparticle physics*, 1st ed., Springer, 2005.

[2] A. K.-H.Kampert,
"Extensive Air Showers and Ultra High-Energy. Cosmic Rays: Historical Review",
History and Philosophy of Physics (2012) 44.

[3] F.G.Schröder, *Instruments and Methods for the Radio Detection of High Energy Cosmic Rays*, 1st ed., Springer, 2012.

[4] Particle Data Group, K. Nakamura et al., "Review of Particle Physics",
J. Phys. G 38 (2014) 090001, URL: `http://pdg.lbl.gov`.

[5] "University of Minnesota. Webpage of a project: "The KAKE Cosmic Ray Telescope"" (),
URL: `http://mxp.physics.umn.edu/s07/projects/s07\_cosmicraysdistribution/index\_files/page0002.htm`.

[6] W.R.Leo, *Techniques for Nuclear and Particle Physics Experiment*, 2nd ed., Springer, 1994.

[7] C.Gruppen, *Detektorphysik*, 2nd ed., Addison-Wesley, 2004.

[8] A. welding supply company inc., "Gases and Equipment" (Accessed at 19.11.2014),
URL: `http://www.advancedweldingsupply.com/gas\%20guide.html`.

[9] B.K.Lubsandorzhiev, "On the history of photomultiplier tube invention",
Beaune Conference on New Development in Photodetection (2006).

[10] HAMAMATSU, "Photomultiplier tubes. Basics and Applications.", *Handbook* (2007) 323.

[11] Wikipedia, "Fotomultiplicator" (Accessed at 19.11.2014),
URL: `http://nl.wikipedia.org/wiki/Fotomultiplicator`.

[12] J. T. F.Karstens A. Stifoutkin, "Performance Tests of the ZEUS Straw-Tube Tracker",
Nuclear Science Symposium Conference Record, 2005 IEEE vol.2 (2005) 1122–1126.

[13] S.Goers, "The Straw-Tube Tracker of the ZEUS-Dtector at HERA",
IEEE Instrumentation and Measurment Technology Conference (2004).

[14] S.Fourletov, "Straw tube tracking detector (STT) for ZEUS",
Nuclear Instruments and Methods A535 (2004) 191–196.

[15] M. M.Traxler Palka et al., "128 channel high resolution TDC with integrated DAQ-system",
Nuclear Instruments and Methods (2005).

[16] "HPTDC. High Performance Time to Digital Converter.", *Handbook* (2004) 102.

[17] M.Traxler, and the others, "128 channel high resolution TDC with integrated DAQ-system.",
Handbook (2004).

[18] D. Hebecker, “STYX Kalibration und Inbetriebnahme”,
Bachelor Thesis: University of Bonn, 2012.

[19] M. Blaut, “STYX Kalibration der Driftzeitverteilungen mit generierten Signalpulsen”,
Bachelor Thesis: University of Bonn, 2014.

List of Figures

List of Tables

Acknowledgements

I would like to express my deep gratitude and respect to Professor Dr. Ian C. Brock for giving me a chance to prove myself, for giving me an opportunity to work in his group and for his patience and motivation through all the times of research and writing this thesis. Also I own him a big gratitude for allowing me to go to many conferences, workshops and research travels which allowed me to gain necessary knowledge for my thesis. And, of course, a great thanks for teaching me how to play Kegeln.

I also want to thank Thomas Velz for his constant programming support and teaching me all I know now about programming. I also would like to offer my special thanks to Jan Stillings and Ozan Arslan for advising me on STYX and for interesting physics discussions, but also on many other topics. And, of course, a special thanks goes to Steffen Schaepe for explaining electronics to me and how to make a Feuerzangenbowle.

I want to thank my colleagues: Rui Zhang for being a good friend from the first day, Anjishnu Bandyopadhyay and Sebastian Mergelmeyer, Irina Cioara, Maike Hansen, Pienpen Seema and Regina Moles-Valls for our girly talks about eFlowRec, unfolding, likelyhood and statistics. I would like to thank Marius Blaut and Henry Axt for showing me that teaching is not such a bad thing and can be fun and educational.

My big thanks goes to my family and friends who never give up on me and always provided their unlimited understanding and support. Christian Wahl and Deborah Elsen for being there through all the years at the university. Thanks to Alex Meringov for his love, for believing in me unconditionally and always listening to my complains at the end of the day.

Thank you!